NTNU – Trondheim
Norwegian University of
Science and Technology

Organic Electrolytes for Thermoelectric Devices and CNT Electrode functionalization by Nitrogen-doping

Ida Hjorth

Nanotechnology
Submission date: June 2012
Supervisor: De Chen, IKP

Norwegian University of Science and Technology
Department of Chemical Engineering

Abstract

In this thesis a thermoelectric cell is developed. Aligned Carbon Nanotubes and aligned Nitrogen-doped Carbon Nanotubes are used as electrode materials. $K_3Fe(CN)_6$/ $K_4Fe(CN)_6$ and Tetrabutylammonium Nitrate (TBAN) electrolytes have been tested for thermoelectric performance, with the two different electrode materials. It was found that Nitrogen doping of CNT's enhances reaction kinetics of the Ferro/Ferricyanide redox reaction. It is suggested that there will be an ideal level of doping, where the electron transfer rate is maximized.

TBAN showed the highest open circuit voltage, but it was discovered that TBAN in dodecanol was unsuitable as an electrolyte for thermocells due to low conductivity and unstable current. The current decreased to less than 1 μA in some seconds.

The highest thermoelectric efficiency obtained was for a symmetric NCNT electrode configuration, with the Ferrocyanide redox couple. The efficiency was 0.007 % of the Carnot efficiency, which is less than state-of-the art electrolyte thermocells. The lower efficiecy was due to non-optimized electrodes and current leakages in the test cell.

Dense, uniform and aligned CNT's were grown on Aluminum foil but using a pre-deposited 2 nm layer of iron catalyst. Ammonia annealing was required before CVD. The treatment with ammonia lead to longer catalyst lifetimes and better alignment. Lengths up to 110 μm was obtained, 15 nm in diameter.

Growth of aligned N-doped CNT's on Aluminum was done using a floating catalyst. Up to 1.5 % incorporation of Nitrogen was achieved.

Sammendrag

I denne masteroppgaven er det utviklet en termoelektrisk celle. Elektrodematerialet er basert på Karbon nanorør og Nitrogen-dopede Karbon nanorør. To forskjellige elektrolytter er testet for termoelektrisk ytelse: $K_3Fe(CN)_6$/ $K_4Fe(CN)_6$ og Tetrabutylammonium Nitrat (TBAN). Nitrogen-doping av Karbon nanorør forbedrer elektrodens reaksjonskinetikk for reduksjon og oksidasjon av Ferro/Ferricyanid. Det er foreslått et det finnes et ideelt doping-nivå, som maksimerer elektronoverføringen.

TBAN i dodecanol produserte høyest spenning, men var upassende som elektrolytt pga meget lav konduktivitet og ustabil strøm. Strømmen sank til under 1 μA i løpet av noen sekunder.

Den høyeste termoelektriske effekten ble oppnådd for symmetriske Nitrogen-dopede Karbon nanorør-elektroder med Ferro/Ferricyanid som elektrolytt. Effektiviten var 0.007 % av Carnoteffektiviteten, hvilket er mindre en de høyeste effektivitetene oppnådd for denne elektrolytten, i litteraturen. Årsaken er blant annet ikke-optimalisert elektrodestørrelse og feilkilder i forbindelse med målinger.

Tettpakkede, opplinjerte og uniforme Karbon nanorør ble grodd på Aluminiumsfolie, ved å deponere et 2 nm lag med jern, oppvarming i en ammoniakk-holdig atmosfære og CVD med Eten som Karbonkilde. Opp til 110 μm lange rør ble oppnådd, 15 nm i diameter.

Vekst av opplinjerte, N-dopede Karbon nanorør på Aluminiumsfolie ble gjort med en flytende katalysator-metode. Opp til 1.5 % Nitrongen inkorporasjon i nanorøret ble oppnådd.

Preface

And hereby I am educated. 5 years ago I had never heard about nanotechnology, now it is my Master's degree. Throughout the years I've learned what is special about small things. And in the end it is the small things that matter in life.

The following pages are my master thesis. Although my chemistry skills were put to a test, I feel I got interesting results throughout this project. It has been interesting and challenging. Most of all, I've learned alot. Those persons I would like to say thanks to, are those who have learned me practical methods in lab; Juan Du and Fengliu Lou. Aknowledges also goes to my supervisor De Chen for good discussions. I've also appreciated the staff at NTNU Nanolab for providing great training and facilites.

Ida Hjorth
MTNANO
Trondheim, June 2012

Contents

Chapter 1

Introduction

The worlds energy consumption is shooting sky high, and there is a hectic activity to meet the rising demand. Technologies for exploitation of gas, oil, coal, wind-, hyrdo- and solar power are being developed with success. Oil, gas and coal are the most important sources of energy. The chemical energy stored in these materials are transduced to work by combustion in a heat engine. The Carnot theorem states the upper limit for the efficiency η_{max} of a heat engine:

$$\eta_{max} = 1 - T_L/T_H$$

T_L and T_H are the temperatures on the cold and hot side, respectively. The average Carnot efficiency for a car engine is less than 35 %. It is estimated that the average efficiency for fuel cells, heat engines, etc. is 40 %, while 60 % of the energy used becomes waste heat, which is low grade energy. Heat is the largest energy source.

Low grade energy is difficult to utilize, transport and store. In general, heat is low grade energy. Thermoelectricity research has experienced a rebirth over the last 20 years [1] due to the energy situation. Heat is the largest energy source. Questing sustainable utilization of heat is a cruical part of investigating new energy sources. There is a range of other, new applications that can utilize the thermoelectric effect: Integration into low power electronic devices such that small low-energetic components can be run by thermopower, or applications in harsh environments. *In vivo* applicaitons are also possible. A thermocell does not need maintenance and can run contiunously powered by body heat. Inplantable medical divices as pacemakers are today powered by batteries that must be replaced in invasive operations. If a pacemaker can use thermopower, the patient does not need to experience repetative operations to replace the battery. The thermocell as power source for implantable sensors is also a possible application.

Thermal energy is directly converted to electrical energy, which is much easier to store and transport. The thermocell advantages are a simple design, possible

Material	S_e mV/K	ZT	η	Ref.	Year
BiSbTe	0.23	1.4	-	[7]	2008
Silicon nanowire	0.4	1	-	[8]	2008
$Fe(CN)_6^{-3/-4}$	1.43	10^{-2}	1.4 %	[9]	2010
$Fe(CN)_6^{-3/-4}$/KCl	1.5	$58 \cdot 10^{-6}$	0.5%	[10]	1994
$Cu(ClO_4)_2$ + silica	1.09	-	0.1%	[11]	1992
Shark gel	0.29	0.0003	-	[6]	2004
TBAN + dodecanol	7.16	10^{-3}	-	[12]	2011

Table 1.1: Thermoelectric materials, their Seebeck coefficient S_e, Figure og Merit ZT, and some experiemental efficiencies (relative to the carnotcycle). The relative efficiency for solid materials can be 20 %

continous operation, it is CO_2-free and needs less maintenance as there are no moving parts[2]. The thermocell can be used to utilize temperatures under 120^{o}C, and can therefore revolutinize the energy marked.

Thermoelectricity is the origin of a voltage due to a temperature difference, and the effect is found more or less in several types of materials. The Seebeck coefficient S_e is the proportionality factor of voltage V and temperature difference dT; V = S_edT. Among solid state materials, the metal alloy Bismuth Telleride and some Semiconductors are applied thermoelectic materials. Their Seebeck coefficients S_e are around 100 μV/K. As the mentioned materials can have high conductivity, the figure merit (ZT) of these materals can be in the range 0.1-3. Materials with ZT from 1 and above are initeresting for pracitical applications. State of the art materials today have ZT up to 3.

One of the best efficiencies achieved by solids are 20 % of the Carnot efficiency [3], *i.e.* ca 5 % [4, 2]. Improvement of efficiencies are mainly sought by reducing phonon contribution to thermal conducivitiy. Nanostructures and grainboundaries scatter phonons and reduce the thermal conductivity. Some simulations found theoretical ZT's up to 15 [5], but this material is not fabricated. Nanostructured thermoelectric devices are costly to fabricate, and it is interesting to investigate cheaper concepts.

Thermoelectricity is also seen in electrolytes. A simple sketch of the concept of an electrolyte based thermocell is shown in figure 1.1. Electrolytes can have much higher S_e than solids, aqueous electrolytes up to 1-2 mV/K and organic or gel electrolytes can have even higher S_e: up to 10mV/K. Thermoelectricity is also seen in nature, several animals have sensory systems that are sensetive to electric fields and temperature, especially marine animals as the shark [6]. Table 1.1 shows some interesting thermoelectric materials and their merits.

The concept of the themrocell has been known a decade, but low efficiencies has discouraged extensive research and development. The maximum efficiency

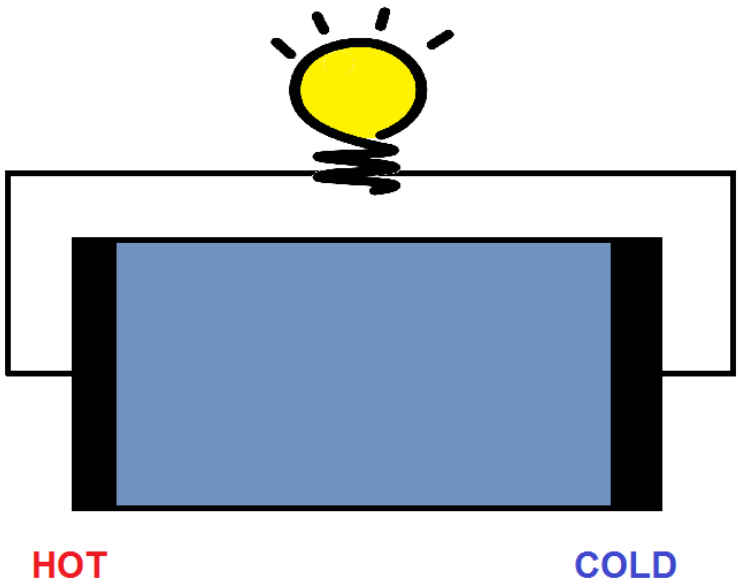

Figure 1.1: Concept sketch of an electrolye based thermocell. The temperature difference of the electrodes gives rise to a voltage.

achieved for solid materials are by now ca 20 % of the Carnot efficiency, while for aqeuous electrolytes it has for a long time been less than 1 % of the Carnot efficiency. Some reserach groups have refreshed the enthusiasm for electrolyte based thermocells. Electrolyte thermocells can be much cheaper to fabricate than nanostructured solid materials.

Baughman et. al. is investigating Carbon Nanofibres as electrode material [9, 3]. Carbon nanotubes (CNT's) are cheap materials compared to other electrode materials, *e.g.* platinum. They have a high specific surface area, which is excellent for electrode applications. The most common electrolyte used in thermocell research is the Ferro/Ferricyanide redox couple, as it has a high S_e compared to other aqueous electrolytes. *Baughman et. al.* showed that efficiencies up to 1.4 % of the Carnot efficiency can be obtained. G*uenoun et. al.* found new electrolytes with even higher Seebeck coefficients [12], such that higher V_{oc} can be produced. These electrolytes are based on organic materials. They have not been tested for thermoelectric performance.

The greatest losses in a thermoelectric cell is high electrical resistance in the electrolyte and low electron transfer rate at the electrodes. Functionalization of large surface area electrodes will increase the current. Vertically aligned carbon nanotubes (ACNT's) are "perfect electrodes" as they have a large accessible specific surface area, and can have high electrical conductivity. However, carbon materials are chemically inert and relatively hydrophobic. Buckypaper is employed more often in the case of thermocell research, as it is easier to synthesize. The advantages of ACNT's are better electrical contact with the electrode support and a more direct access for the electrolyte to the surface. CNT's can be functionalized to catalyze the electron transfer, i.e by Nitrogen doping (NCNT's). These defects can improve the reactivity of the tubes. A very recent paper, published february 28 2012, discussed the effect of doping with Nitrogen or Boron [13], and they showed that Nitrogen doping can improve electron transfer rates, but they did not show an overall improvement of performance when the electrodes was tested in a thermoelectric cell.

Further work to improve the efficiency of an electrolyte based thermocell will include the quest for, and engineering of electrolytes with high Seebeck-coefficients, in the range 10-100 mW/K. This will increase the open curcuit voltage and compensate for losses by low conductivity. An improvement of reaction kinetics at the electrodes is also an important area of focus. Functionalization by doping with Nitrogen should be further investigated.

The main advantage of the electrolyte based thermocell is the low fabrication cost compared to solid materials. ACNT's can be grown on cheap substrates as household aluminum foils. Aluminum have high electrical and thermal conductivity, which makes the suitable for thermocell substrates. The melting temperature of aluminum is only 660 ^{o}C. This limits the growth temperature. Successful growth

of ACNT's by CVD on Al has been obtained. Doping of CNT's with Nitrogen can be done in CVD, but most synthesis temperatures are for this are above 700^{o}C. To my knowledge, there are no reports on Nitrogen doping of ACNT's on Al foil, or substrates grown in similar temperatures.

This master project will develop a termoelectric cell with ACNT-based electrodes. Two different electrolytes will be tested. The conventional Ferro/Ferricyanide couple and an organic electrolyte with higher S_e. The project involves several steps that has not been done before: (1) ACNT's are grown on Aluminum foils with predeposited Iron as catalyst and Ethene as carbon source. (2) Growth of Aligned Nitrogen-doped CNT's (NCNT's) below 700^{o}C (3) Testing of the termoelectric performance of an organic electrolyte with high S_e. (4) Testing of the performance of aligned N-doped CNT's.

The goal of this project is to study the effect on current densiy and overall cell performance when using ACNT electrodes functionalized by N-doping and to compare the performance of the organic electrolyte vs. the conventional $Fe(CN)_6^{-3/-4}$.

Chapter 2

Theory

2.1 Thermoelectricity

Electrochemistry involves an electrical circuit coupled to an electrode and electron transfer from/to the electrode to/from the electrolyte. Oxidation of the electrolyte occurs at the anode, reduction at the cathode. The energy released during this process can be used as electrical work, and corresponds to the change in free energy Δ G of the redox reaction. Considering the half reaction $A^+ + e^- \rightleftharpoons A$, the potential E of this half cell is described by Nernst equation.

$$E = E^0 - \frac{RT}{nF} ln \frac{a_{red}}{a_{ox}} = -\frac{\Delta G_r}{nF}$$

E^0 is the standard state potential relative to the standard hydrogen electrode (SHE), a is activity and for low concentration the expression can be simplified by using concentrations rather than activities. R is the gas constant, the potential E has units Volts, n is the number of electrons transferred in the balanced reaction, F is the Faraday constant. The potential is temperature dependent, the temperature dependence

$$\frac{\delta E}{\delta T} = -\frac{1}{nF} \frac{\delta \Delta G_r}{\delta T} = \frac{\Delta S_r}{nF}$$

ΔS_r is the entropy of the reaction. The first theoretical basis for the thermoelectric effect was developed by Eastman [14], nearly a century ago. The theory is based on open circuit conditions. There is no model for thermocells which deliver current or takes overpotentials into account[10].

Concidering a full cell with an electrolyte where there is a temperature gradient. The concentration at the cold electrode will be higher than the concentration at the hot electrode as species diffuse towards the colder regions. This is called the "Soret effect". In an electrolyte, Soret equilibium may take days to establish

and the Soret effect can sometimes be neglected. Electrons in conductive and semiconducting solid materials will also exhibit a similar but more rapid effect called the Seebeck effect, where electrons diffuse from warm regions to cold regions, creating an electrical field. The voltage arising between two nodes with different temperatures is porportional to the material's Seebeck coefficient.

$$dE = S_e dT$$

. This expression is also valid for thermocells using electrolytes. The Seebeck coefficient S_e has it's origin from gain in entropy at the higher temperature by electrode reaction, and entropy by transport of species fromt the cold to the hot regtion, $\overline{S}$.

$$nF\frac{dE}{dT} = \Delta S_r + \Delta\overline{S} = S_e$$

Calculations shown in *Guenon et al.* [12] show that

$$S_e = \frac{\sum_i q_i n_i \hat{S}_i}{\sum_i q_i^2 n_i}$$

q is the charge of species i, n is the number and $\widehat{S}$ is the "Eastman entropy of transfer", meaning

$$\hat{S} = \overline{S_i} - s_i$$

$\overline{S_i}$ is the "transported entropy" by particles transporting heat and s_i is the partial molar entropy. Important contributions in to the Eastman entropy is the interaction between ion and solvent. Solvent molecules tend to orient such that electrostatic forces reduce the overall energy, *e.g.* water molecule dipoles in the hydration shells. The degree of local orderering of solvent molecules around the ion is an important parameter for Eastman entropy of transfer.

In table 1.1 the Seebeck coefficients for some substances are shown. The Seebeck coefficients of electrolytes are higher than those for solid materials, but their conductivitues are much lower. To compare the thermoelectric power, the figure of merit ZT is representative.

$$ZT = (\frac{dE}{dT})^2\sigma/k$$

σ is the electrical conductivity of the electrolyte and k is thermal conductivity. $\frac{\sigma}{k}$ for metals and semiconductors are around 10^4 KS/W, while electrolytes can be around 30 KS/W. ZT should be close to or above 1 for practical applications.

2.1.1 Thermocell efficiency and power

The current in a thermoelectric cell is provided by redox-reactions at the electrodes. The magnitude of the current depends on reaction kinetics, active electrode surface area and concentration of ions at the surface.

The power conversion efficiency of a thermocell is

$$\eta = \frac{V_{oc} I_{sc}}{4Ak(\Delta T/d)} = \frac{S_e j_{sc} R_T}{4} \tag{2.1}$$

where V_{oc} = open circuit voltage, I_{sc} short circuit current, A area, k thermal conductivity and d electrode separation. R_T is thermal resistance, j is current density. A convenient measure of the thermal cell efficiency is the efficiency relative to the carnot efficiency. The maximum power $P_{max} = V_{oc} I_{sc}/4$.

2.2 Heat transfer

Transfer of heat is transfer of energy. Steady state heat conduction is described by Fourier's law

$$\vec{Q} = -k\nabla T \rightarrow Q_x = -k_x \frac{dT}{dx}$$

Where Q is the heat flux, k is the thermal conductivity of the material, T is temperature. Thermal resistivity is the reciprocal of thermal conductivity. The total heat resistance is the resistivity multiplied with the length of the device, in the case of an electrolyte: R_T = d/k, d is the separation of the electrode.

In solids, heat transfer is conductive, while in fluids transfer of heat happens by conduction and convection. Convection is bouyant motion of warm fluids, as the density of a liquid decreases with temperature warm fluid flows up. When k is low, hence conductive heat transfer is small, convective heat transfer will dominate.

In a liquid electrolyte all species contribute to heat transfer, while only the ionic species contribute to electrical conduction. In a metal the electrons are the major heat carrier.

2.3 Electrolyte-Electrode interface

When a metal or a semiconductor is in contact with and electrolyte, electrons are injected into or extracted from the solid material as the chemical potential of the electrons must equalize. The surface of the material is then charged. The electrostaic force attracts ions and orient polar molecules as water. Molecules can also be adsorbed to the surface because of Van der waals interactions. Two models are used to describe to concentration of ions and potential drop near the interface: The simple Helmoltz model, where ions form a compact layer at the surface and the Guy-Chapman model, considering the thermal motion of ions which will create a diffuse double layer. Figure 2.1 a) shows a combination of these two models. The concentration at the electrode surface is described by

$$c_{si} = c_{0i} e^{z_i \phi F/RT}$$

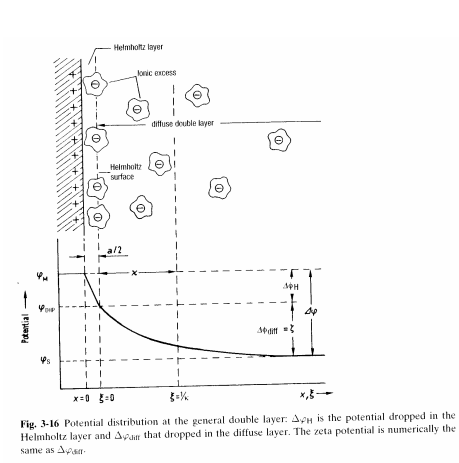

Fig. 3-16 Potential distribution at the general double layer: $\Delta\varphi_H$ is the potential dropped in the Helmholtz layer and $\Delta\varphi_{diff}$ that dropped in the diffuse layer. The zeta potential is numerically the same as $\Delta\varphi_{diff}$.

(a) Electrical double layer

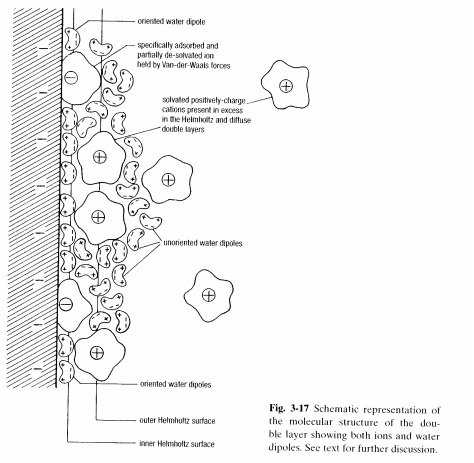

Fig. 3-17 Schematic representation of the molecular structure of the double layer showing both ions and water dipoles. See text for further discussion.

(b) Specific adsorption because of van der Walls interactions

Figure 2.1: Sketch of different interactions between a solid surface and electrolyte: Compact helmholtz layer, diffuse double layer and molecules adsorbed because of van der Waals interaction. These figures are adapted from "Electrochemistry"[15].

The concentration of species i at the surface and in the bulk is is c_{si} and c_{oi}, z_i is the valency and the potential difference form surface to bulk is ϕ. The thickness of the double layer depends on ionic strenght and bulk concentration. High ionic strength and high bulk concentration reduces the double layer thickness. Molecules can also be adsorbed on the surface by van de Waal's interactions. Such a situation is shown in figure 2.1 b), where anions are adsorbed to a negative electrode[15].

2.4 Electrolytes

The electrolytes used in this project are Tetrebutylammonum Nitrate (TBAN) solvated in 1-dodecanol and equimolar Potassium Ferrocyanide and Ferricyanide solvated in water. Their chemical formulas are shown in figure 2.2. TBAN is a quaternary amine bonded to four alkyl groups. The oxidation state of TBAN is independent of pH. TBAN is a common surfactant. Solubility in water is less than 2mg/mL. The thermal conductivity of 0.1 M TBAN in dodecanol is 0.169 W/mK.

In Ferrocyanide the oxidation state of Iron is 2+. The oxidation state of Iron in Ferricyanide is 3+. Iron is octahedrally coordinated by 6 cyano-lignads. Thermal conductivity is affected by concentration, but in this project the thermal conductivity is assumed to be similar to that of water, 0.58 W/mK.

The Seebeck coefficients of both electrolytes are given in table 1.1.

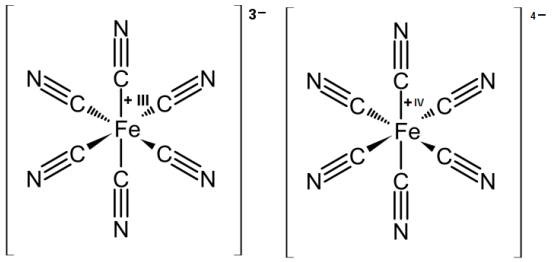

(a) Ferro/ferricyanide

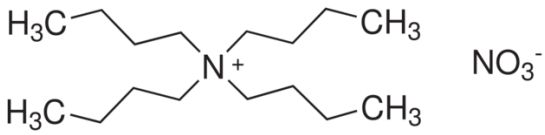

(b) Tetrabutylammonium Nitrate

Figure 2.2: Chemical formulas.

2.5 Carbon Nanotubes

Carbon nanotubes are rolled up graphene sheets. In the graphene structure Carbon hybridization is sp^2, and the π electrons are dislocated over the entire structure. CNT's are chemically and electrocehmically inert[16]. CNT's have high specific surface area, which makes them interesting as support materials for catalysis and as electrodes. They can be semiconducting with a small bandgap or metallic, depending on chirality. Single walled nanotubes have diameters up to 1-2 nm, and nanotubes reasonably wider than this are multiwalled. Mulitiwalled nanotubes are usually metallic, as at least on of the walls should have a rolling vector in the metallic regime. The separation between each wall is ≈ 3.4Å.

Nitrogen doped CNT

Nitrogen doping of CNT's changes electrical, chemical and structural properties of the CNT. A unique bamboo-structure is often seen [17], this bamboo-strucure has a high number of edge defects etc, as shown in figure 2.3. There are different types of bonding of the N-atom to the C-atoms in the CNT, these are also shown in figure 2.3. The binding energies are around 400 eV. Each bonding type have different properties. The pyridinic type gives the semiconduction tube a metallic character due to the introduction of electron donor levels[18]. The pyridinic Nitrogen increases bascicity[19] and catalyzes base catalyzed reactions due to a localized lone pair. The pyrrolic type leads to a structural change as a pentagon is introduced. The characteristic bamboo structure is the caused by the pyrrolic Nitrogen. For both types, the 2p-electrons contribute in the π-electron system re-

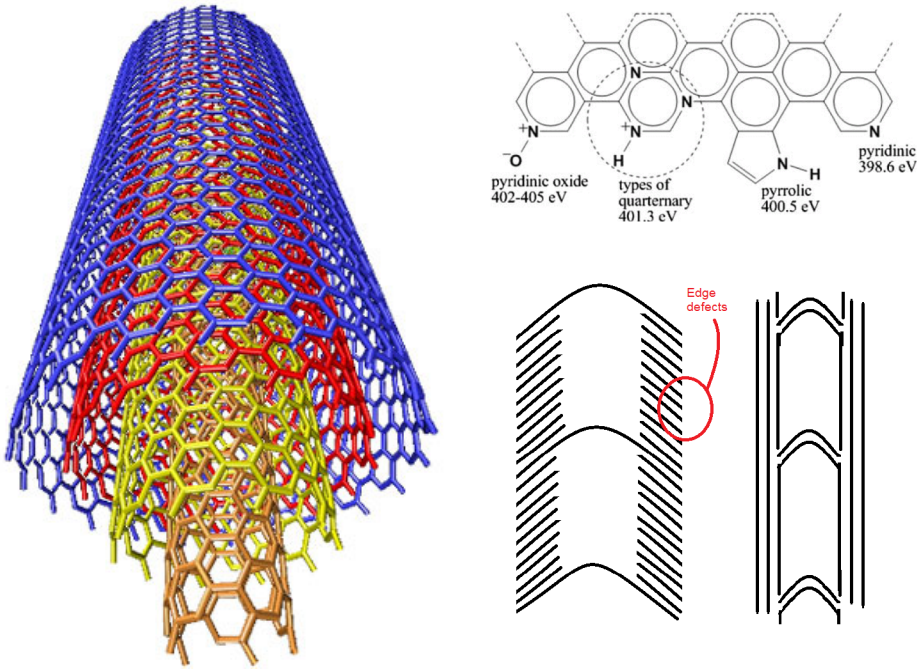

Figure 2.3: Multi-walled CNT (left). Binding modes of N in CNT (top right). Simple sketch of the bamboo structure, with and without edge defects (bottom right).

sponsible for electric conductivity. The substitutional Nitrogen is quaternary and contributes to the π-system. At low concentrations and for semiconducting chiralities, the substitution introduces a chemically active localized energy level[20]. It has been reported that N-doping of CNT's improve hydrophilicity[21]. For high N-incorporation the pyrrolic sp^3 binding is more abundant than pyridinic sp^2[22].

Most N-doped CNT's are synthesized above 700 ^{o}C, but there are also a few reports in N-doping at lower temperatures. Ammonia or Nitrogen containing carbon sources are used in CVD. Commonly, 0.5-10 % N is incorporated.

Chemical Vapor Deposition

CNT's are often synthesized by Chemical Vapor Deposition (CVD). Gasous carbon containing species are decomposed on a catalyst. Common gases used as C-source are CO, C_2H_2, C_2H_4, C_2H_6, CH_4 and ethanol. Common catalysts are nanoparticles of iron, nickel and cobalt. First, the carbon source is adsorbed onto the catalyst and decomposed. From there, there are two suggested growth mechanisms. (1) The C-atom can solvate in the catalyst particle and diffuse thorough it, driven by a temperature gradient or a concentration gradient. (2) The C-atom can diffuse on the surface of the catalyst. There are two growth modes, base and tip growth. These are sketched in figure 2.4. In base mode, the catalyst particle remains supported by the substrate, and the CNT grows upwards, while in base mode the nanotube is supported by the substrate and pushes the catalyst particle upwards as it grows. There are indications that the wetting properties of the catalyst particle is correlated to the growth mode, where tip growth can be seen when the interface energy between the substrate and catalyst is high [16].

The catalyst is deposited either before CVD, or in-situ as with the floating catalyst method. Pre-depsition methods can be by evaporation or sputtering of a thin metal layer, which can give a smooth film and good thickness control. This is desirable, as the tube diameter is often related to the catalyst particle size. During heating the thin film cracks into small nanocrystals. Ostwald ripening can occur, giving a non-uniform set of catalysts.

In the floating catalyst method, the catalyst is solvated in a solution, i.e. ferrocene in ethanol. The solution in injected into the CVD reactor with a carrier gas. In this case, ethanol is the carbon source.

For aligned CNT growth, catalyst uniformity is important, as it is the "crowding effect" which gives aligned tubes[16]. Aluminum foil is an interesting substrate as it is cheap. One article reports growth of aligned CNT's on aluminum foil [24], using electron beam evaporation to deposit iron, and CVD with ethanol as C-source. Aluminum melts at 660 ^{o}C, which restricts synthesis temperature. Common temperatures for CVD is 600-1000^{o}C.

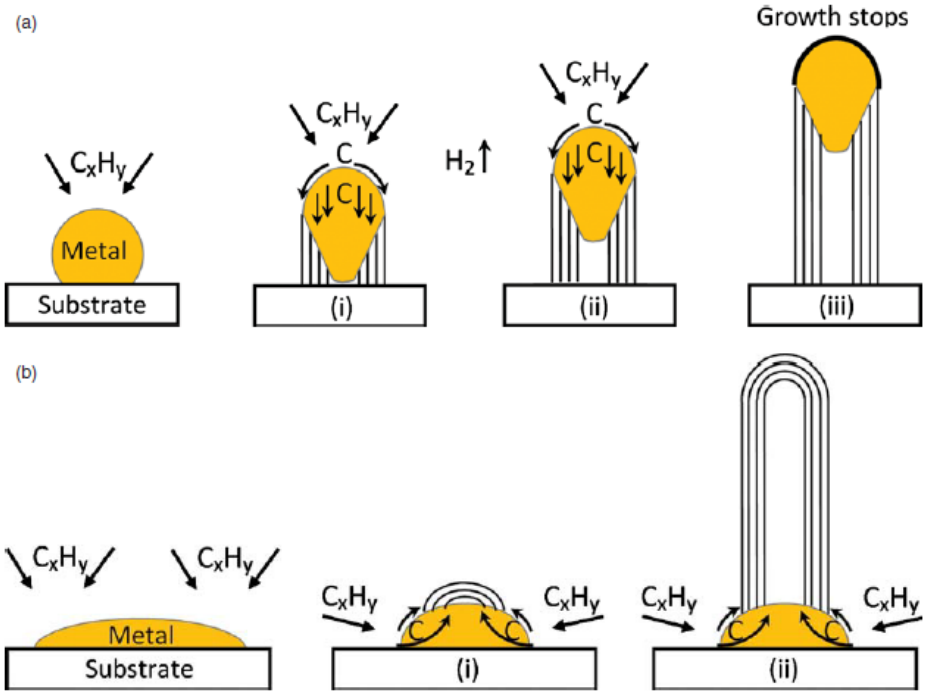

Figure 2.4: CVD of hydrocarbons to grow nanotubes. Tip-growth (a) and base growth (b). Carbon is transported via surface diffusion or by solvation into the catalyst particle and percipitation. Adapted from [23].

2.6 Reaction kinetics

Wether the reaction A + B $\rightleftharpoons$ C will occur is predicted by the change in free energy. The change in free energy, the driving force for the reaction does not account for the reaction kinetics. The kinetics is assessed in "transition state theory". The species A and B will for a "transition complex" which have higher energy. From this transition state the reaction can proceeed to C, or go back to distinct A and B. The increased energy of the transition state is the energy barrier A and B must cross to form C, and the height of the energy barrier E_a determines the reaction rate k.

Figure 2.5 (left) sketches the reduction in activation energy E_a for a reduction reaction, when an electical field is applied. β is the symmetry factor, and when β=0.5 the electrode interacts equally with both reductant and oxidant. The figure to the right shows how a catalyst can change the activation energy. Enzyme catalysis often follow such behaviuor where there are several "quasi-stable" intermediates. The catalyst can have a much simpler behaviour also, just by reducing the height of E_a in one step.

The rection rate k follows

$$k = Ae^{E_a/RT} \tag{2.2}$$

where A is a constant, R is the gas constant and T is temperature. This eqiation is called the Arrhenius equation.

2.7 Characterization techniques

2.7.1 Scanning Electron Microscopy

In Scanning Electron Microscopy (SEM) an electron beam scans a sample while a signal is being collected. The signal can be back scattered electrons (BSE), secondary electrons (SE) and also X-rays. Secondary electrons are those electrons emmited by the sample when they are excited by the electron beam. The X-rays are used for element mapping in EDX and have their origin from de-excitation of electrons bound to an atom, and are characteristic for an element. SE are used to form an image that can show the morphology of a sample, while BSE are useful to find heavy elements in the sample as heavy elements backscatter electrons more easy than light elements.

2.7.2 X-ray photoelectron spectroscopy

X-ray photoelectron spectroscopy (XPS) is based on the photoelectric effect: An x-ray beam interacts with a material such that the material emitts electrons. These electrons are collected. By measuring the energy of the electron, the bonding energy of the electron to the atom in the sample can be found, as

$$E_{binding} = E_{photon} - E_{kinetic} - \Phi$$

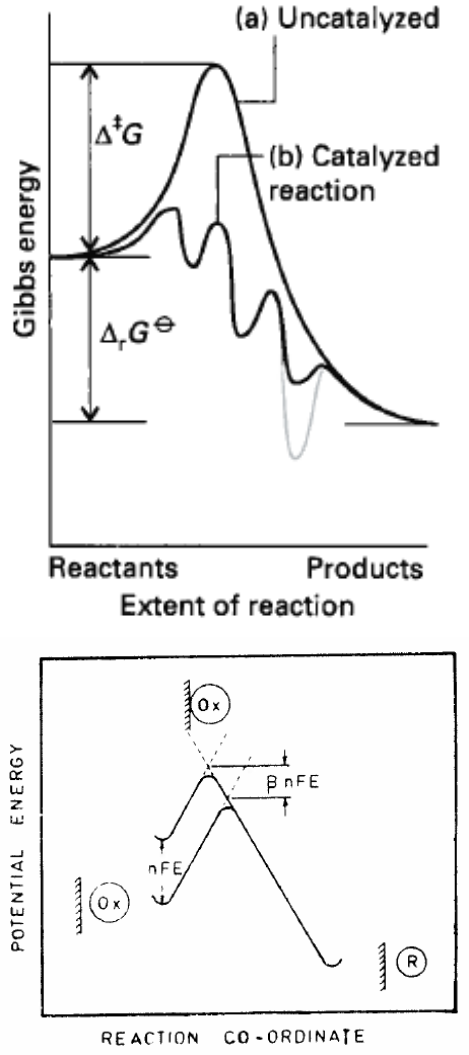

Figure 2.5: The lowering of activation energy for a reduction reaction by an applied electrical field (bottom). Adapted from [25]. The lowering of the activation energy by a catalyst (top). Adapted from [26].

Φ is the work funciton of the detector. The bonding energy of an electron to an atom depends on the orbital in which the electron is.

2.7.3 Cyclic voltammetry

In Cyclic Voltammetry a periodic potential is employed on the working electrode and the current response is measured. As the potential is increased and it reaches the potential for oxidation to occur, and anodic peak current will arise. In a mass tranport limited reaction, the current is porportional to the ionic flux J towards the electrode. The flux follows Fick's diffusion law as seen in equation (2.1). The expression for current will be as shown in (2.2), where I is current and A is electrode area. Cottrell related this expression for current with time, and this expression is given (2.3). c_0 is the bulk concentration. His solution assumes a planar, uniformely accessible and smooth electrode.

As the oxidation or reduction occurs, a concentration gradient depending on time t will occur near the electrode, as seen in figure 2.6. The maximum concentration gradient is when the concentration at the electrode reaches zero. Randles found the expression for current as a fuction of time for a linear voltage sweep[27]. For fast reaction kinetics, the peak current is proportional to the square root of the swipe rate, equation (2.4).

Considering a system with slow reaction kinetics, the maximum consentration gradient point ($c_{x=0} = 0$), x=0 is at the electrode surface, will occur later than for a pure mass transport limited system, and E_p, the potential at which I is max will be higher.

$$\frac{\delta c_i(x,t)}{\delta t} = D_i \frac{\delta^2 c_i(x,t)}{\delta x^2} \tag{2.3}$$

$$J = -D\frac{\delta c}{\delta x} \Rightarrow \frac{I}{nF} = -D_i A \left[\frac{\delta c_i(x,t)}{\delta x}\right]_{x=0} \tag{2.4}$$

$$I = nFAc_0\sqrt{D/\pi t} \tag{2.5}$$

$$I_p \propto \sqrt{D_i v} c_i A \tag{2.6}$$

A typical graph is shown in figure 2.6. The voltage is swept linearly from V_{min} to V_{max} and then it is reversed back to V_{min}. During the reverse swipe, there will be a reduction current in the same fashion as oxidation current. This cycle can be repeated multiple times. The "capacitive current" is related to the reversion of the electrical double layer.

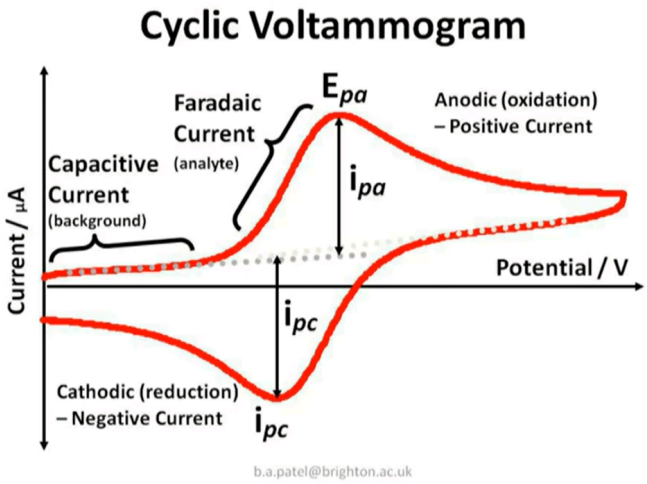

Figure 2.6: Typical current-voltage curve for a cyclic voltammety scan.

Chapter 3

Experimental

In this diploma project ACNT's, and Nitrogen-doped ACNT's have been synthesized using two different CVD-methods: by pre-deposition of iron catalyst on an Aluminum substrate and by the floating catalyst method. Characterization of the tubes includes studies in SEM and XPS. The synthesized materials are used as electrodes in a thermoelectric cell, and the performance of the cell is tested with two different electrolytes: Aqueous Ferro/Ferricyanide and TBAN in dodecanol.

3.1 Synthesis of ACNT's

ACNT's were grown using Aluminum foil as a substrate. An iron catalyst was thermally evaporated on the substrate before CVD.

Catalyst deposition

Thermal evaporation of iron was performed in NTNU Nanolab, an ISO 7 cleanroom. 8 μm thick Aluminum foil substrates was washed with isopropanol and blown dry with N_2. A Cressington 308R Evaporator with quartz crystal balance mass controller was employed. The iron source was 99.95 % purity iron from Kurt J Lesker company loaded in a Tungsten boat. The Al substrate was mounted on the sample holder with heat resistant tape. The system was pumped to 10^{-5} torr. Rotation of the sample holder and water cooling was activated. The current through the tungsten boat was increased from 0 to 210 A (60 %) in 6-8 minutes. Evaporation onto the substrate started when the shutter covering the iron boat was removed. Evaporation occured at a rate $\approx$ 0.1 Å/sec. 2 nm and 4 nm thick layers was deponated. Evaporation was stopped by covering the iron boat with the shutter and slowly decreasing the current to zero. Watercooling and rotation was switched off and the chamber was vented. Finally, the substrate was taken out of the chamber, cut into suitable pieces and kept in a plastic box.

	Ar	H_2	C_2H_4
a	160	20	20
b	160	7	20
	t(anneal)	t(grow)	T(grow)
c	30	45	640, 650
d	30,10	120	650
e	30,13	120,110	660

Table 3.1: CVD gas flows mL/min, annealing and growth time in minutes, growth temperature (at reactor wall) in Celsius.

Chemical Vapor Deposition ACNT's

The CVD system used is sketched in figure 3.1. Ar, H_2 and C_2H_4 gas flows was controlled with mass flow controllers while the flow of ammonia was controlled with a rotanometer. A thermocouple was placed at the reactor wall, in the center of the oven. The sample was placed on a quartz plate and placed in the center of the oven. The tube inner diameter is 4 cm, while the oven length was 35 cm.

The chamber was heated 20 K/min to the growth temperature in either a Ar/H_2 or Ar/NH_3 atmosphere. The wall temperature T_{wall} was either 640 ^{o}C, 650 ^{o}C or 660^{o}C. Table 3.1 shows some of the CVD conditions that was tested: Combination of gas flows and combinations of of temperature, growth time and annealing duration.

After the desired growth duration, the supply of ethene and hydrogen was stopped. The ractor was passively cooled down.

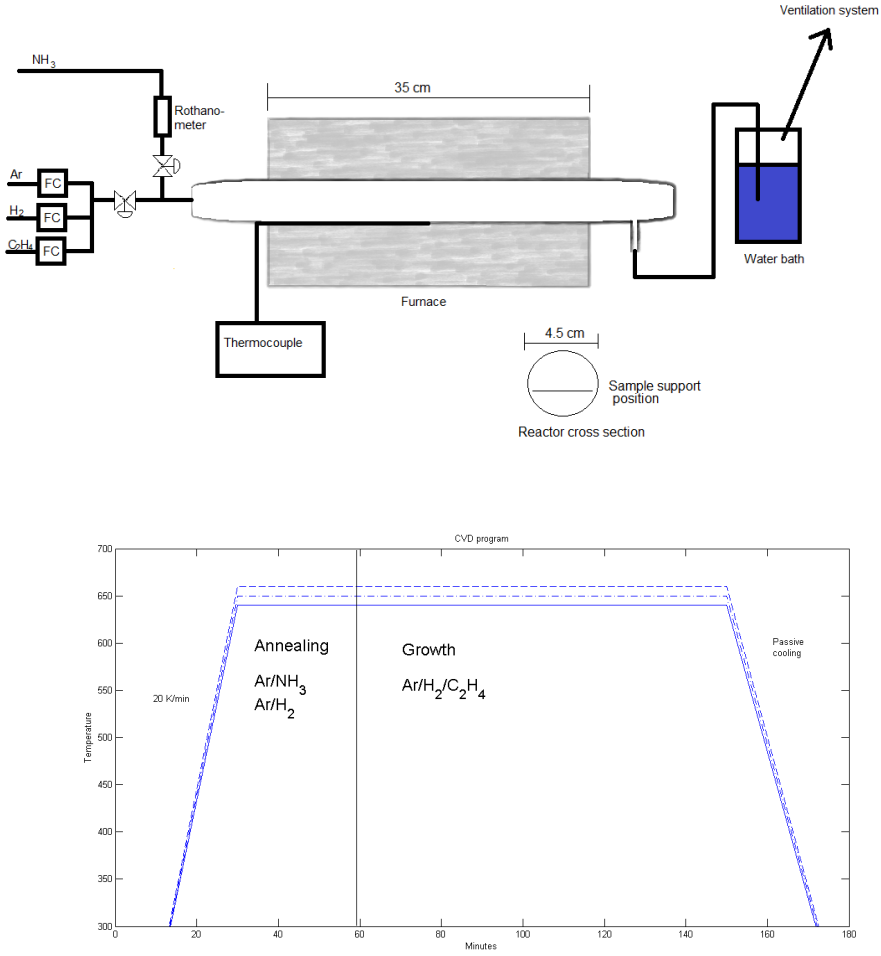

Figure 3.1: System for CVD on pre-deposited catalyst and temperature programme.

Sample	Ar	H_2	NH_3	x(NH_3)
1	210	15	0	0
2	170	15	40	0.18
3	130	15	80	0.36
4	0	15	135	0.90

Table 3.2: Gas flows and total injected volume of catayst for floating catalyst synthesis of NCNT's. Gas flow units are in mL/min.

3.1.1 N-doped aligned CNT's

Nitrogen doped ACNT's (NCNT) was synthesized using a floating catalyst method. The CVD setup is shown in figure 3.2. The reactor was heated 20 K/min up to 620 ^{o}C, and then 2 K/min to 640 ^{o}C, in an Ar/H_2 atmosphere. At 640 ^{o}C NH_3 was added to the gas flow, and the catalyst was deposited *in situ*, by injection of a 0.05 M solution of ferrocene in ethanol for 30 minutes. Ethanol is the C-source. The injection rate was 20 mL/min. NH_3 is used as N-source. The amount of hydrogen gas was held constant at 15 mL/min, while the amounts of Ar and NH_3 in the carrier gas was varied. Table 3.2 shows the different composition of gases that was tested.

3.2 Thermoelectric cell

A device for testing the thermoelectric performance of different electrodes and electrolytes was designed as shown in figure 3.3. The electrodes was mounted on Aluminum support plates with carbon tape. The inter-electrode separation is 2.2 cm. The Aluminum plates also seprates the middle compartment from the two end pieces. The full piece was held together by steel screws, insulated with electrical insulating tape.

Electrolyte is injected into the middle compartment with srynges through the brown tubes. A second srynge in the second brown tube is used to ensure the compartment is full and also to seal the cell. Thermocouples are inserted into the electrolyte between the Aluminum plates and the teflon mid-piece, to measure the temperature at the electrode-electrolyte interface. V_{oc}, I_{sc} and Resistance is measured by coupling the Aluminum supports to a multimeter. The resistance between the steel screws and the alumunum plate was measred to ensure they were electrically insulated. Resistances between the screw and plate that was larger than 1 Mω was accepted.

The cold electrode is cooled by passing cold water thourgh the end compartment, while hot electrode is heated by pumping hot water though the other end compartment. A FLUKE 83 multimeter and FLUKE 51 thermometer has been used.

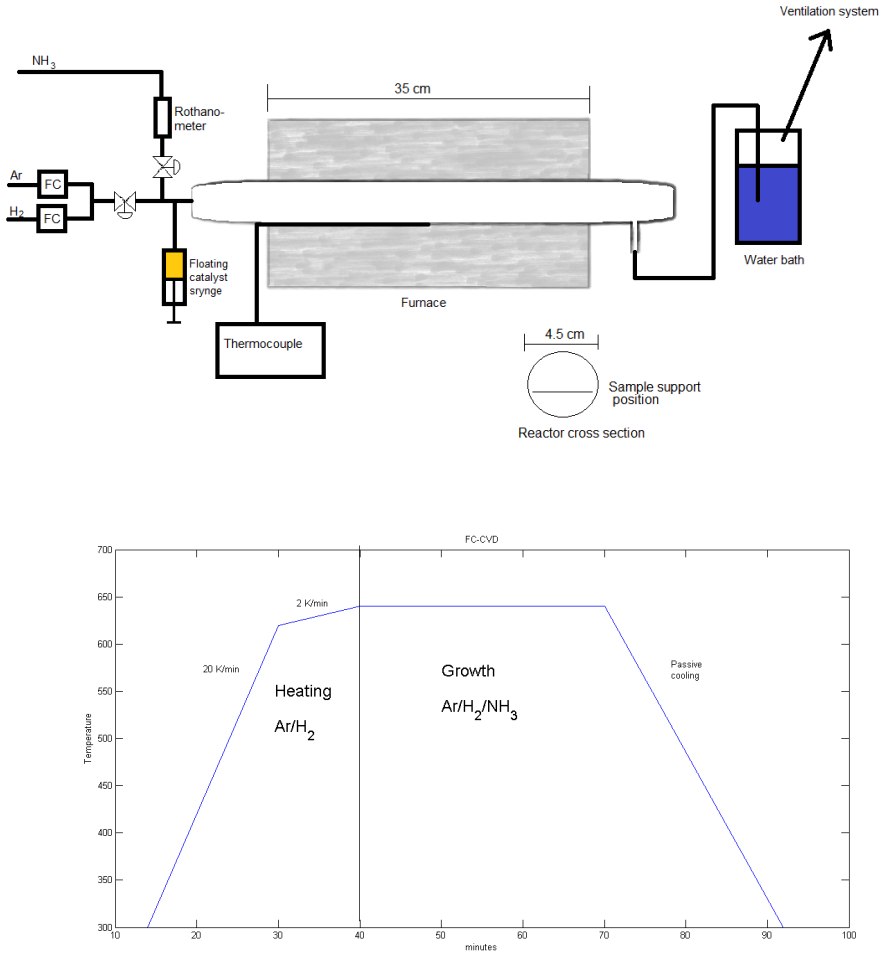

Figure 3.2: Floating catalyst set-up and CVD program.

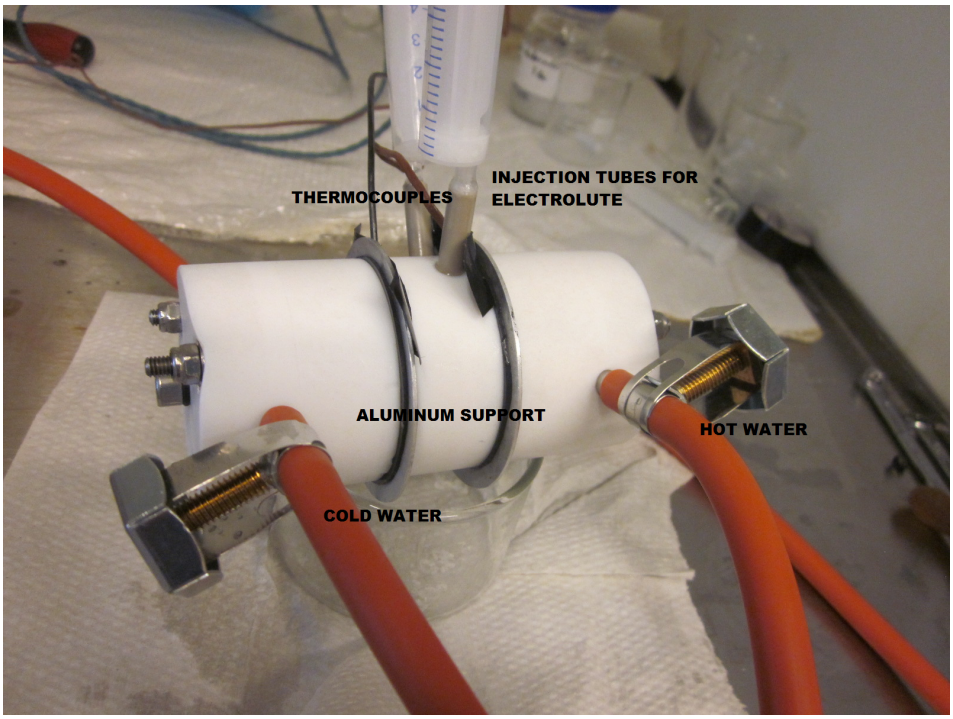

Figure 3.3: Device for testing of thermoelectric performance. Electrode separation is 2.2 cm.

3.3 Characterization instruments

CNT's are characterized with SEM to find tube lengths, diameters, size distribution and alignment. XPS is used to characterize doping levels in NCNT's, but quantitatively and qualitatively with regards to binding mode. Cyclic voltammetry is used to determine reaction kinetics of NCNT vs CNT electrodes.

SEM Hitachi S-5500 in-lens S(T)EM, with a cross-section holder is used for all SEM images of ACNT's.

XPS XPS belonging to Prof. Steinar Raaen at institue of Physics, NTNU.

Cyclic Voltammetry A versaSTAT MC system from METEK and Versastudio software have been used for Cyclic Voltammetry testing. The projected electrode area is 0.38 cm^2, and the separation between working electrode, Ag/KCl reference electrode and Pt counter electrode has been constant for all CV-tests. The electrodes have been mounted on a titan support with carbon tape. The Ag/KCl potential was 0.2 V compared to SHE.

Chapter 4

Aligned CNT's

Aligned CNT's and aligned NCNT's is used as electrode material, and these were grown by CVD. The catalyst was deposited on the substrate prior to CVD or by the floating catalyst method during CVD.

4.1 CVD on pre-deposited catalyst

Growth of aligned CNT's on Aluminum foil was performed as described in the experimental chapter; substrate preparation by thermal evaporation of iron on Aluminum foil, and growth by CVD using ethene as C-source.

Substrate preparation

Iron was deposited by thermal evaporation. 2 or 4 nm was deposited. After the substrate was taken out of the evaporation chamber, the colour changed quickly to a reddish-brown tone. Iron oxide, more popular called "rust" has this colour, which means that the nanolayer of iron is oxidized.

The deposited thickness was monitored with a quarts crystal mass controller, using the tooling factor given by the producer. The tooling factor is used for calibration of the mass controller, it might be inaccurately calibrated. The real thickness can be controlled i.e. with AFM, but layers as thin as 2 nm are not easy to characterize, especially as the surface of Aluminum foil itself isn't smooth. It will be difficult to deconvolute what is iron and what is the substrate. Therefore, calibration is as given by the producer.

Annealing atmosphere

When the heating of the substrate for CVD was done in an Ar/H_2 atmosphere there was no or very trace Carbon formation on the Al foil. When the samples was

heated and annealed in Ar/NH_3 atmosphere, there was aligned CNT formation. The duration of annealing showed to be significant for the lenght of the CNT's, this will be returned to in subsection 4.1.1.

The iron catalyst oxidized quickly and iron oxide has low catalytic effect. H_2 is a reducing agent [28] for iron oxide. Still, when the substrate was treated with hydrogen for 2 hours there was no CNT growth. It is assumed that 2 hours is more than sufficient to reduce the iron oxide, as the vast litterature on this topic does not show that such long periods with annealing is required.

ACNT's have previously been grown in similar fashion on Aluminum foil with iron as catalyst, deposited by electron beam evaporation. No additional treatment with hydrogen was done, but the group used ethanol as C-source[24]. When ethanol is decomposed, a OH-radical is formed, and this OH-radical reacts with amorphous carbon[23]. Formation of excessive amorphous carbon contributes to catalyst deactivation [29, 30]. Formation of amorphous carbon and rapid deactivation of the iron catalyst might be the reason the attempts to grow ACNT's with Fe catalyst on Aluminum using only $Ar/H_2/C_2H_4$ gases did not succeed.

The effect of annealing the substrate in an Ammonia atmosphere is interesting. Several papers claim that Ammonia promotes formation of uniform catalyst nanocrystals[31, 32], by some sort of etching effect. Another effect is formation of FeN. The effect of FeN is not clearly understood, but it is suggested that it reduces the amount of amorpohus carbon and prevents deactivation [33, 34]. CNT's were formed when the substrate was pre-treated by annealeing for 10-30 minutes in Ar/NH_3 (160 mL/min,80 mL/min), before CVD.

Considering the growth mechanism where Carbon atoms undergo surface trasport, and using a model proposed by Jourdain et. al. [35], there are three important steps in CNT growth: (1) Mass transport of precursors to the catalyst surface, (2) adsorption and dissociation of the precursor which is thermally activated, and (3) "defect anneling", i.e. incorportation of disordered surface carbon to the ordered carbon nanotube network. Defect annealing is also thermally activated. Catalyst self-deactivation happens when step 2 is much faster than step 3. Considering Iron and Iron Nitride in this project, the first was quickly deactivated while the latter has a much longer lifetime in same conditions.

Surface segregation of Nitrogen in FeN has been found [36]. Nitrogen reduces the surface enegry, which can also be intepretated as a reduction in reactivity. This will reduce the decomposition rate of hydrocarbon, and then the growth rate. The growth rate of CNT's on FeN in this project is much slower than the growth rates on iron found in the vast litterature. However, this is no more than a discrete indication that the growth rate and dissosciation rate on FeN is slower, as no direct comparision can really be done because temperature, substrate and C-source will greatly affect the growth rate.

The energy barrier for incorporation into the CNT lattice might be affected by

the strength of adsorption to the catalyst, when the adsorption to the catalyst is weak the energy barrier for incorporation can be low. The reduction in surface energy by nitride formation indicates that the barrier for incorporation is lowered.

Hence, for pure Fe step (2), dissosciation, is fast while step (3), incorporation into the CNT lattice is slow, while for FeN step (2) is slower and step (3) is faster. Therefore FeN conserves activity for a longer period.

It was experienced that the ACNT's grown by pre-treatment of Fe on Aluminum foil is easily scratched off the surface. The adhesion is less good than the adhesion of tubes synthesized by the floating catalyst method. This is a drawback for the application of this synthesis method, as the electrodes are difficult to handle without skratching off tubes.

Role of H_2

Growth of CNT was attempted with C_2H_4:H_2 = 1:1 and 3:1. Only scarce CNT formation was observed when the ratio was 1:1. It is widely accepted in litterature that hydrogen improves catalyst activity by preventing formation of amorphous carbon by reducing decomposition of the carbon source on the catalyst[37]. This means that catalyst deactivation by Carbon saturation should not be the cause for growth inhibition when the hydrogen/ethene ratio is 1:1.

Hydrogenation of C_2H_4 into Ethane or adsorbed C-atoms into methane can happen when H_2 is adsorbed on the catalyst surface. This effect can be postive, i.e. removing Carbon from the surface to avoid deactivation, as observed in the litterature. At high partial pressured of hydrogen this effect competes with growth of CNT's. The catalyst surface will be covered with hydrogen, inhibiting adsorption of ethene and inhibiting CNT formation. The lowering of hydrogen partial pressure from 1:1 to 1:3 was followed by formation of CNT's, meaning that hydrodrogen adsorption is no longer dominating.

Catalyst film thickness

CNT's grown on a 2 nm and 4 nm thick catalyst layer shows different morphology. The latter resulted in poorly aligned CNT's with a wide diameter distribution, see figure 4.1. A thicker film can be less uniform, giving catalyst particles with different size. As the diameter of the catalyst often is correlated to the tube diameter, tubes with different diameters are formed. Also, catalyst particles with different size might have different kinetic behaviour. Reactivity often increases with decreasing size [38], and small nanoparticles will have higher kinetics than large particles. When tubes grow at different rates, the alignment will be less good, as alignment is a "crowding effect".

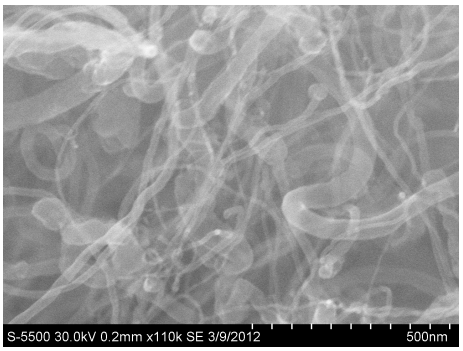

(a) 4 nm catalyst thickness

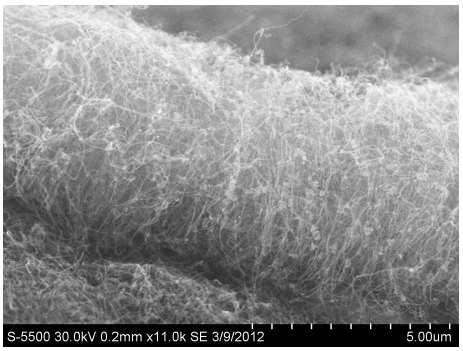

(b) 4 nm catalyst thickness

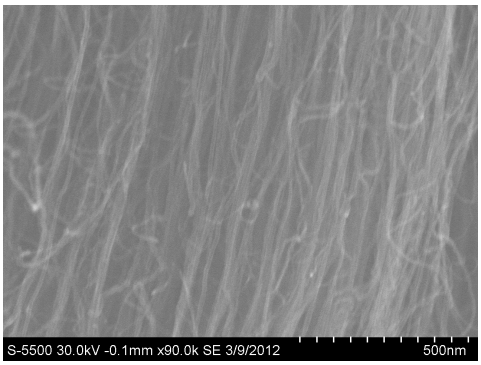

(c) 2 nm catalyst thickness

Figure 4.1: SEM images of CNT's grown on Aluminum foil substrates with thermally evaporated iron catalyst layers, 2 or 4 nm. The growth conditions are the same: 30 minutes annealing and 3:1 ethene:hydrogen at 640°C.

	T_{wall}	Anneal time	Growth time	Length	Diameter
1	640	30	45	6	7
2	650	30	45	6.5	15
3	650	30	120	50.8	15
4	650	10	120	20	12
5	660	30	120	110	13
6	660	13	107	60	15

Table 4.1: CNT morphology and growth parameters. Temperature in ^{o}C, length in μm, average diameter in nm and time in minutes.

4.1.1 Growth conditions and morphology

ACNT's was grown successfully with 160 mL/min Argon, 20 mL/min C_2H_4 and 7 mL/min H_2 at 640-660^oC after annealing with Ammonia for 10-30 minutes. The iron film thickness was 2 nm. The temperature at the reactor wall T_{wall}, the duration of annealing in NH_3/Ar atmosphere and growth duration was varied. Table 4.1 shows the resulting tube length and diameters.

Both annealing time and growth temperature affects reaction kinetics. Sample 1 and 2, grown in 45 minutes are 6 and 6.5 μm respectively. By increasing the wall temperature 10 degrees, the raction rate has increased 8 %. Sample 3, grown for 2 hours at 650^{o}C is 50 μm long. This means that the growth rate is noninear, but much faster the second hour than the first hour. It is common for the growth rate to initially increase, and decrease after a while when the catalyst starts to deactivate[39], but these changes in in growth rate are for a much smaller time scale than the presented experiments. The presented experiment seemingly has a rather long "incubation time" before growth rate ramps up. The exact nature of the development of the growth rate cannot be deciphered from the two datapoints above and more thorough studies should be performed if a clear understanding of the process is desired. The growth model suggested in section 4.1 is simplified and cannot account for the "incubation time".

Sample 3 and 5 are grown at T_{wall} = 650 and 660 ^{o}C, but otherwise the parameters are the same. The length of the tubes in sample 5 are twice the length of the tubes in sample 3. The 10 ^{o} increase in temperature yields a great increase in growth rate. It is known that the CNT growth rate can change rapidly close to the optimum growth temperature[39]. The temperature was not increased further to avoid melting of aluminum.

When the annealing time is reduced from 30 to 10 minutes the tube length decreases from 50 to 20 μm. One explaination can be that longer annealing times yields more iron nitride and a postponed catalyst deactivation.

But it was also seen that in shose samples with shorter annealing times, sample 4 and 6, nanotube curling occured, see figure 4.2 c) and d). The tubes grown with 30 minutes anneling pre-treatment had better alignment, 4.2 a) and b). Curling

of ACNT's was studied by Chen et. al. [40], and they found that curling of CNT's lead to a reduction in growth rate due to diffusion limitations. Sample 4 and 6 are substantially shorter than their fellow samples 3 and 5, synthesized at 650 and 660^{o}C respectively. Sample 4 and 6 were annealed for a shorter time than sample 3 and 5, it seems as there is a correlation between annealing, curling and reduction in growth rate. It is said that curling can be a result of difference in growth rate, as difference in growth rate leads to less alignment and friction between tubes. As it is claimed that Ammonia can etch the catalyst particles such that more uniform catalyst particles are obtained, it seems that after 30 minutes annealing there is a more uniform set of catalyst particles than after after 10 minutes. Hence, growth rate is related to curling, which can be correlated to the uniformity of catalyst particles, which is affected by the degree of annealing in ammonia.

A selection of SEM pictures are shown in figure 4.2. One problem with characterizing tube diameter in SEM is out-of-focus tubes and astigmatism. Blurred tubes will seem wider than their real size and astigmatism can make tubes seem both wider and narrower. Approximate measurements of diameters is done, and it is seen that the diameters of sample 2-6 are in the same range: 12-15 nm. Therefore it is assumed that the density of the ACNT's are similar.

4.2 Nitrogen doped ACNT's

Nitrogen doped ACNT's was grown by the floating catalyst method and characterized with SEM and XPS. The weight gain was measured, and the tube length and diameters characterized with SEM. The weight gain, tube length and diameter is presented in figure 4.3 e) and table 4.2. The un-doped sample (210 mL/min Ar, 15 mL/min H_2) has most weight gain, around 10 %, and longest tubes (14μm). When partially replacing Ar with NH_3, the weight gain decreases to 1 % and tube length to 4.3μm (x(NH_3) = 0.18). Furhter, when the fraction of ammonia is increased at the cost of Ar, the weight gain stabilizes around 3 %, and tube lengths are 3 μm (x(NH_3) = 0.35) and 1.7 μm (x(NH_3) = 0.9). Three SEM picutres are shown in figure 4.3. The alignment is less good than the alignment seen for most of the CNT samples synthesized by pre-deposition of the catalyst, seen in figure 4.2.

The tubes synthtesized with x(NH_3) = 0.35 are more uniform than the tubes synthesized with x(NH_3) = 0.9. An approximate density can be estimtad by evaluating the weight gain and tube length, the calculations for this is indicated in Appendix A. This shows that ρ(x(NH_3) = 0.9) = 2.7ρ(x(NH_3) = 0). There is a large uncertainty in the weight measurement, as the mass of carbon is only ca 1 mg.

The first indication on successful N-incorporation in the CNT's is found in the Secondary Electron SEM-images, figure 4.3 c. The twisted tubes resembles the shape of NCNT's with a bamboo-like structure seen in many papers [32, 22], caused by the pyrrolic binding mode. A closer look at these turmoils, figure 4.3 d) shows that

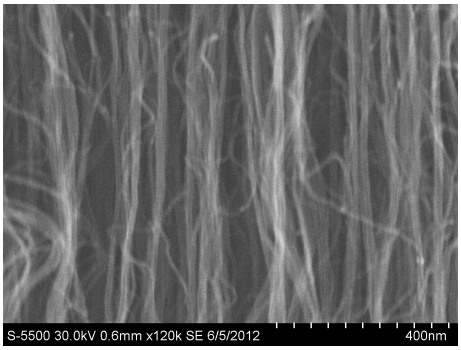

(a) Sample 5: 660^{o}C, 30 min anneal and 2 hours growth

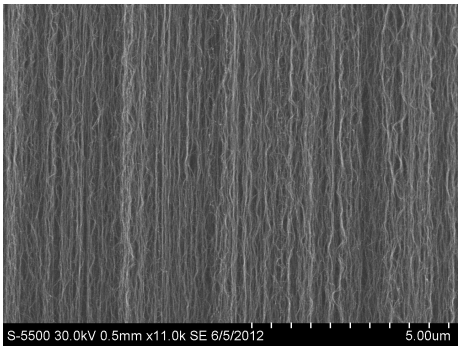

(b) Sample 5: 660^{o}C, 30 min anneal and 2 hours growth

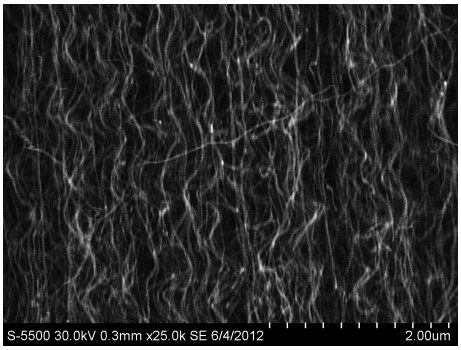

(c) Sample 6: 660^{o}C, 13 min anneal and 1:47 hours growth

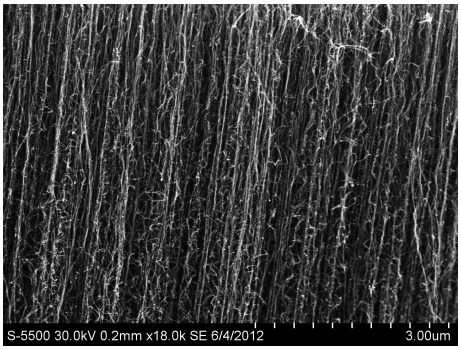

(d) Sample 4: 650^{o}C, 10 min anneal and 2 hours growth

Figure 4.2: CNT's grown after conditions given in table 4.1.

	t [min]	L [μm]	d [nm]	%N	x(NH_3)
1	30	14	16	0	0
2	7:30	5	16	0	0
3	30	1.7	26	1.5	0.9
4	30	3	28	1	0.35

Table 4.2: Tube morphology, FC-CVD grown ACNT's and A-NCNT's.

these tubes have brighter bands at the kinks. The contrast in a SE-SEM image comes from the number of SE-electrons hitting the detector. The topography of a sample is important, as grooves will seem darker as many of the electrons coming from a groove are re-absorbed in the walls around, which is called shadowing. The bright bands may have origin in such a topography effects, and then indicating that the tubes have a wavelike structure. Another origin of contrast is mass: If the wall of the tube is very thin, a large fraction of the beam will not interact with the wall and few SE will be created. The bright bands may indicate a closed inner tube, yielding mass contrast. The bamboo structure has closed inner tubes. The bright bands apearing in figure 4.3 have their origin in mass contrast from closed innter tubes, as the wave structure is unrealstic.

4.2.1 XPS

The samples was studied in XPS to see wether any Nitrogen was incorporated, and to estimate the amount. Thanks to Steinar Raaen, Department of Physics, NTNU for the operation of the XPS. Figure 4.4 shows these XPS spectra: (a) x(NH_3) = 0.18, (b) x(NH_3) = 0.36, (c) x(NH_3) = 0.9, (d) Pre-deposited catalyst. The large and small peak around E = -290 eV is assigned to Carbon, while the N-peak is around E = -400 eV. In (b) and (c) the N-peak is small, but visible. In (a), there is a minimum signal of Nitrogen well buried in the noise. (d) does not show any signal from Nitrogen.

A rough estimate of the N-content is done by integrating the peak intensities of C and N, and comparing the ratio. The sensetivity factor for N is 1.6 compared to C, such the integrated N-intensity is divided by 1.6. For (c) this gives approximately 1.5 % N, and slightly less than 1% for (b). However, these numbers are not fully accurate as the peaks are just slightly above noise level.

The CNT sample prepared by pre-deposition of the catalyst was also checked in XPS. As the substrate was annealed in an ammonia atmosphere before CVD to form FeN, it was interesting to check wether Nitrogen was incorporated into the Carbon lattice. It is assumned that the part of the grown nanotube containing Nitrogen are the segments grown in the initial stage of the CVD process, as the concentration of Nitrogen in the catalyst would have been highest in the beginning. In case of base-type growth, the nitrogen would then exist at the very top

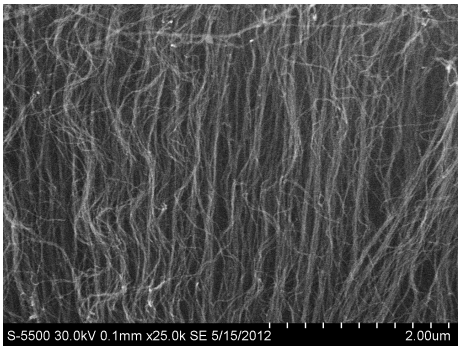

(a) No doping

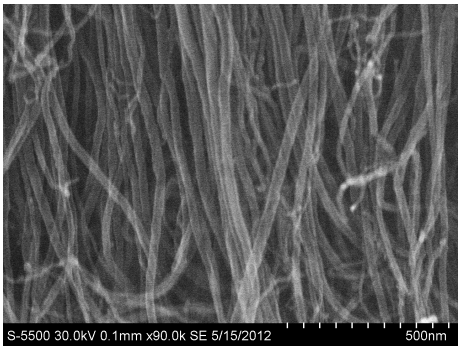

(b) 40 mL/min NH_3, 170 mL/min Ar, 15 mL/min H_2

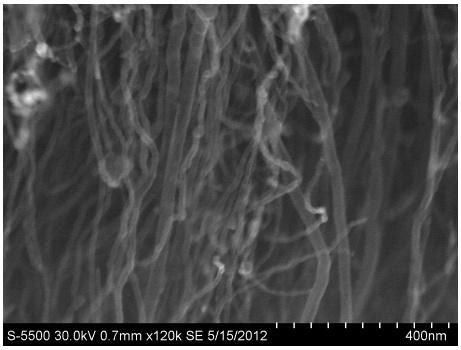

(c) 135 mL/min NH_3, 15 mL/min H_2

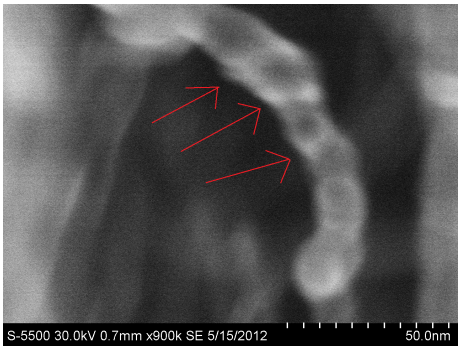

(d) 135 mL/min NH_3, 15 mL/min H_2

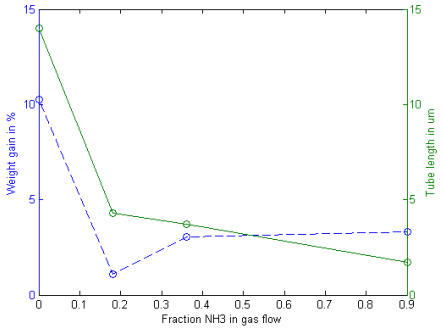

(e) Wegiht gain and tube length

Figure 4.3: SEM pictures of floating catalyst synthsized NCNT's.

surface, therfore within the range of the XPS signal which is approximately the top 10 nm of the surface. The growth mode when using Fe as a catalyst is often base-mode. To assure base-type growth, the BSE-SEM signal was studied. It did not show any trace of high heavy elements at the surface, hence base-mode growth was not disproved. This BSE picure is not shown in the report. Figure 4.4 (d) shows the XPS spectrum for this sample. It does not show any signal from Nitrogen. However, very small amounts of nitrogen ($\ll 1\%$) cannot be resolved in the XPS spectrum. But these low levels of doping might not contribute to reasonable structural changes etc. in the nanotube.

Nitrogen binding mode. By studying the Nitrogen peak carefully, it is seen that the peak consists of overlapping peaks with origin in different hybridizations of Nitrogen: The pyridinic binding (E= 398.6 eV) and pyrrolic (E=400.5 eV), and also the substitutional type (401.3 eV). The pyridinic peak is slightly more intense than the pyrrolic and substituational peak, meaning that pyridinic defects are dominating. This is in agreement with litterature, stating that pyridinic defects dominate at low level doping.

4.2.2 Nitrogen doping

To the best of my knowledge, it has not been reported synthesis of Nitrogen-doped aligned CNT's at temperatures suitable for using aluminum foil as substrate. The XPS spectra in figure 4.4 shows that small amounts of Nitrogen is incorporated, the largest incorportion, ca 1.5 % was achieved with the parameters: 135 mL/min NH_3, 15 mL/min H_2 and injection of 20 mL/h 0.05 M Ferrocene in Ethanol for 30 minutes. The synthesis was not optimized and it is reasonable to believe that higher incorportation of Nitrogen can be achieved. The effect of altering injection rate and gas partial pressures can be investigated. What is observed is that the use of ammonima slows down the growth rate. The higher partial pressure of ammonia, the shorter tubes are grown. Both content of Nitrogen and density of tubes increases with increasing ammonia partial pressure. This is accompanied with increased size distrubution and reduced alignment. The dominating binding mode is the pyridinic mode, in agreement with known research [17].

In the litterature, it is found that the incorporation of Nitrogen ranges from 0.5-10% Nitrogen [41]. The contents achieved here is in this perspective not impressive. However, for many applications a very heavy doping of nitrogen in not desired. Further development of the method for growing N-doped CNT's as described here should aim to control the incorporation ratio of nitrogen, improve growth rate and optimize growth kinetics.

First attempts to improve the method should be by reducing the injection rate of the floating catalyst, as much of it did not react inside the reactor. Also, reducing the total flow volume will give more uniform growth inside the reactor. As Ammonia seem to reduce growth rate, the flow of Ammonia should also be reduced. It was seen that the incorportation of N did not increase more then ca

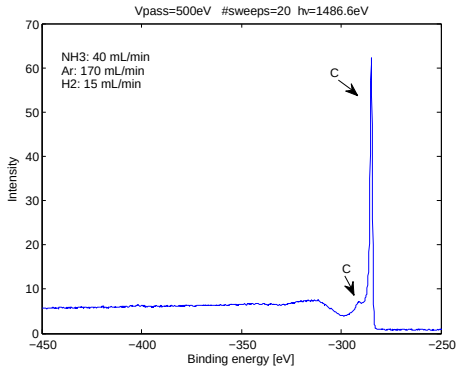

(a) x(NH_3) = 0.18

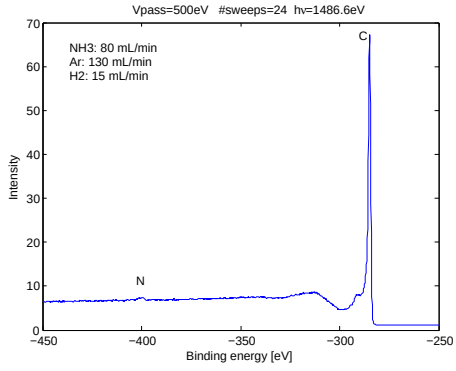

(b) x(NH_3) = 0.35

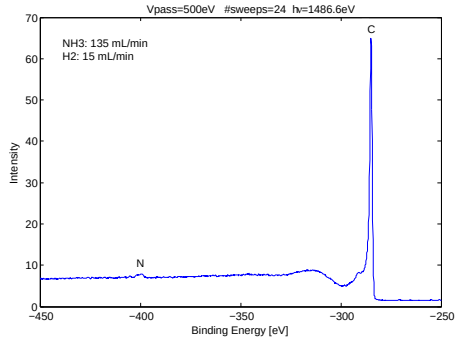

(c) x(NH_3) = 0.9

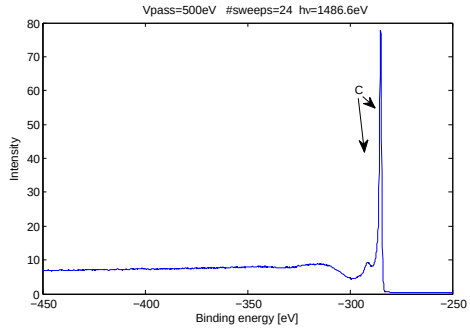

(d) Pre-deposited catalyst

Figure 4.4: XPS spectrum of A-NCNT samples and ACNT grown by pre-deposition of the catalyst.

0.5 % by increasing the partial pressure from 0.35 to 0.9, so reducing the partial pressure of Ammonia does not need to be a trade off with N-incorporation.

Chapter 5

Thermoelectric testing

5.1 Cyclic Voltammetry

An NCNT and CNT electrodes widt different tube lengths were tested in Cyclic Voltammetry. The synthesis parameters and tube length of the electrodes is given in table 5.1. The resulting normalized I-V graphs are found in figure 5.1 and 5.2. 0.4 M equimolar Ferro/Ferricyanide was used as electrolyte. 0.4 M is claimed by *Baughman et. al.* to be the optimal concentration. Two different scan rates v was applied: 0.1 V/s and 0.01 V/s. An Ag/KCl electrode was used as reference. Multiple cycles was performed, to ensure stability. The 5th and last scan cycle is shown.

Overall, the shapes of the graphs have the same characteristics: One anodic and cathodic current peak, confirming that it is the same reaction taking place. However, the position and size of the anodic and cathodic current peaks, E_{pa} and E_{pc}, differ. The numerical difference between E_{pa}-E_{pc} is given in table 5.2 to illustrate the displacement of I_p. The N-doped CNT's have the smallest displacement, and for the CNT samples the anodic and cathodic peaks are shifted to a more positive and negative direction, respectively. The peak separation increases with increasing tube length. The 110 μm CNT samples shows irreversible characeristics

Electrode	Catalyst	T_{growth}	t_{growth}	Gas [mL/min]
NCNT 1.7 μm	Floating	640 ^{o}C	30 min	NH_3: 135 H_2: 15
CNT 5 μm	Floating	640 ^{o}C	7 min	Ar: 210 H_2: 15
CNT 14 μm	Floating	640 ^{o}C	30 min	Ar: 210 H_2: 15
CNT 60 μm	Pre-dep.	660 ^{o}C	1:47 h	Ar: 160 H_2: 7 C_2H_4: 20
CNT 110 μm	Pre-dep.	660 ^{o}C	2 h	Ar: 160 H_2: 7 C_2H_4: 20

Table 5.1: Synthesis parameters for the electrodes tested in CV.

	E_{pa}-E_{pc}		I_{pa}	
Electrode	0.1 V/s	0.01 V/s	0.1 V/s	0.01 V/s
NCNT 1.7 μm	0.54	0.24	0.020/0.032	0.0069
CNT 5 μm	0.70	0.32	0.044	0.01516
CNT 14 μm	0.73	-	0.056	-
CNT 60 μm	1.03	-	0.086	-
CNT 110 μm	N.A.	0.41	N.A	0.0236

Table 5.2: Absolute value of the anodic peak current I_p and the corresponding potential shift illustrated by E_{pa}-E_{pc}. The two NCNT electrodes have slightly different peak currents, 20 and 32 mA.

when v = 0.1 V/s, there is no anodic or cathodic peak. It has reverisble kinetics at v = 0.01 V/s.

The current is normalized with respect to tube length. The tube diameter of the CNT's are similar, as seen in table 4.1 and 4.2, and it can be assumed that the density of the CNT's are similar, both for FC synthesized and when the catalyst is pre-deopsited. The diameters of the NCNT's are larger and more dispersed. The realtive density of the NCNT's with respect to CNT's is calculated by comparing the weigth gain shown in figure 4.3 e), and it was found to be 2.7 times the density of the NCNTs. However, the total mass of the NCNT's is ca 1 mg. Due to the low mass, there will be a reasonable insecurity in the measurement and calculation of density. Therefore the currents are normalized with respect to length, not mass.

It is seen in figure 5.2 that the normalized current is higher for NCNT's than for the compared CNT electodes, and the normalized current decreases with tube length. The absolute magnitudes of the current peaks are given in table 5.2. It is seen that I_p for the two NCNT electrodes differ.

Double layer capacitance. The capacitive current is the linear increase in current before onset of the redox reacion, and corresponds to the capacitance of the double layer. By comparing the slopes of the capacitive current, a ratio of the double layer capacitance for different electrodes can be found. In figure 5.2 b), the capacitive current for the NCNT and 5 μm CNT electrode is fitted linearly. It is found that C_{ncnt}=1.9C_{cnt}. The proof is given in Appendix B. Doping with Nitrogen is an n-type doping, *i.e.* the dopant contributes with an extra electron to the electronic system as Nitrogen has one more valence electron than Carbon. As the number of electrons in the CNT increases, the increased electron density can increase the surface charge and then also the double layer capacitance. The increase in capacitance will depend the level of doping, as the level of dopants affects the number of donated electrons.

Cola et. al. found that the capacitance of the NCNT electrode was 4 times the capacitance of the CNT electrode. The level of doping was 5 %, in consitency with the above theory that double layer capacitance is doping dependent, and that

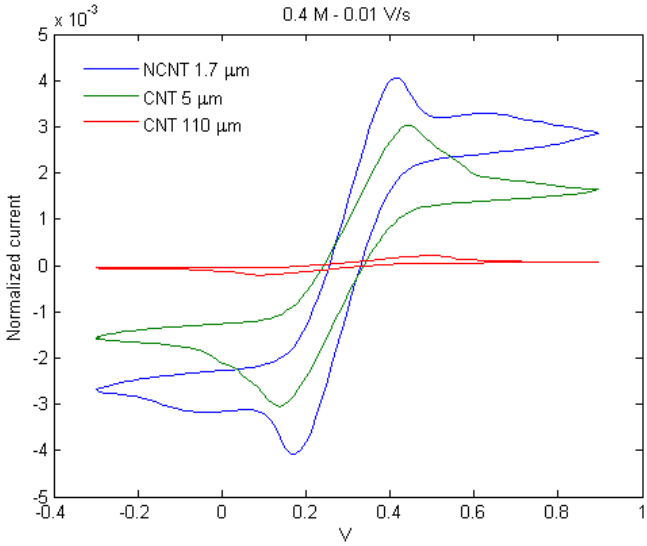

(a) v = 0.01 V/s

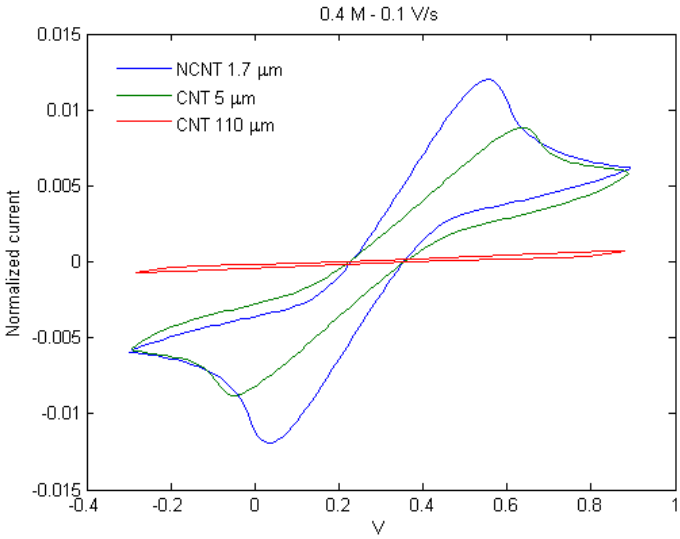

(b) v = 0.1 V/s

Figure 5.1: Cyclic Voltammetry of aligned NCNT and different aligned CNT electrodes in 0.4 M ferro/ferricyanide solution with Ag/KCl reference electrode. The 5th cycle is shown for two different swipe rates v: 0.1 and 0.01 V/s. Normalized with respect to tube length (in μm).

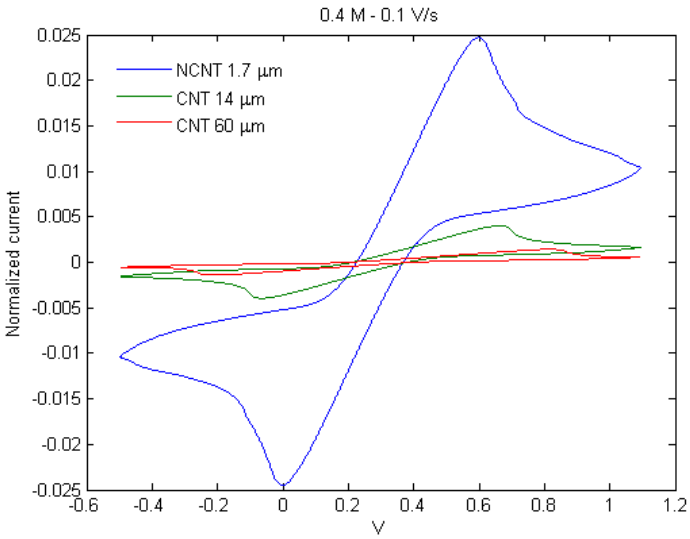

(a) Cyclic Voltammetry of aligned NCNT and different aligned CNT electrodes in 0.4 M ferro/ferricyanide solution with Ag/KCl reference electrode. The 5th cycle is shown for swipe rate v = 0.1 V/s. Normalized with respect to tube length (in μm.)

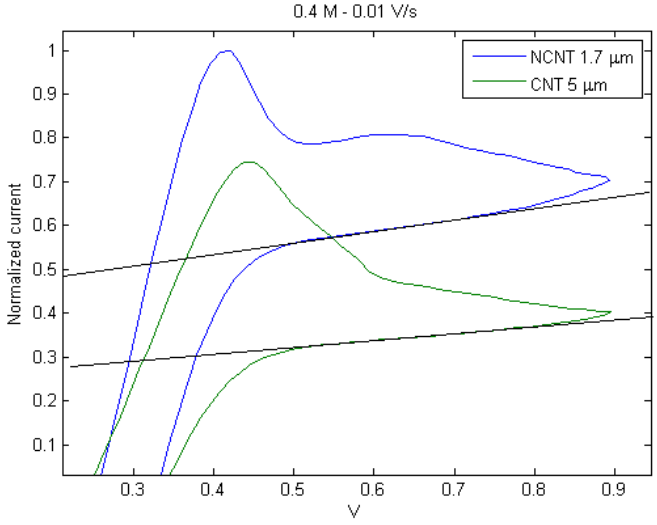

(b) Linear fitting of the capacitive current, v = 0.01 V/s

Figure 5.2: Cyclic voltammetry and capacitance fit.

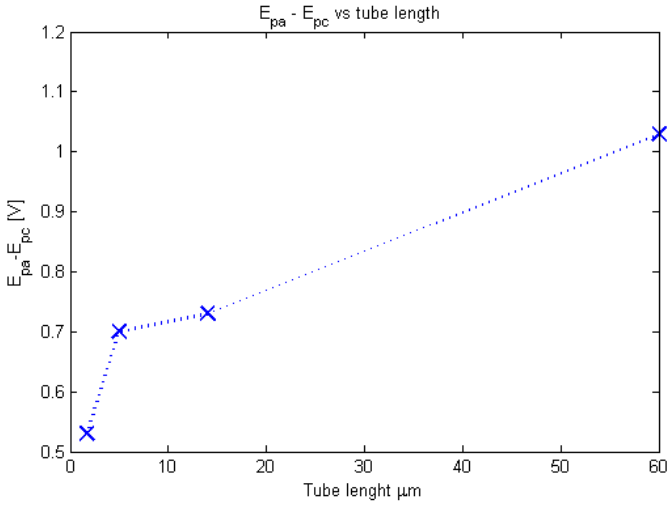

Figure 5.3: E_{pa} - E_{pc} vs tube length, swipe rate 0.1 V/s

the capacitance increases with increased doping.

E_p. Reaction kinetics. Difference in E_p is a representative qualitative figure for reaction kinetics. For slower reaction kinetics, the potential corresponding to the anodic and cathodic current peak will shift to respectively higher and lower values. This means that the reaction kinetics of the NCNT electrode is faster than the kinetics of the CNT electrodes, and the kinetics k slows down with increasing tube length: k(NCNT) > k(5 μm CNT) > k(14 μm CNT) > k(60 μm CNT) > k(110 μm CNT). The shape of the CV curve for the CNT 110 μm sample at v=0.1 V/s in figure 5.1 b) should be commented. It shows irreversible charge transfer characteristics as there is no anodic or cathodic peak, the voltage window is not wide enough for oxidation and reducion to occur because of too slow charge trasfer. When the swipe rate is decreased to 0.01 V/s it shows reversible characetristics.

As there is a correlation between tube length and E_p, the question is wether the fast kinetics of the NCNT sample is due to Nitrogen doping or due to the short tube length, 1.7 μm. In figure 5.3 b), E_{pa}-E_{pc} is plotted versus tube length, for v = 0.1 V/s. The 110 μm CNT sample is not included as it has irreversible character.

The E_p displacement decreases smoothly from the 60 μm to the 14 and 5 μm tubes. Then, there is an abrupt decline in peak displacement for the Nitrogen doped electrode. The difference in length of the Nitrogen doped electrode and the shortest CNT electrode is not so big, but the difference in peak displacement is large compared to the difference between the 5 and 14 μm CNT electrodes. This indicates that the doping effectively enhances reaction rate.

Cola et. al. [13] found that N-doped buckypaper has higher reaction rates than buckypaper in a 0.01 M Ferri/Ferrocyanide solution. They argued that the negatively charged surface of the N-doped electrode leads to a higher potassium concentration at the surface, as given by the Guy-Chapman equation.

$$c = c_o e^{z\phi F/RT} \tag{5.1}$$

From equation 5.1 it is seen that when the potential drop ϕ from the electrode to the bulk is larger, there will be a higher concentration of oppositly charged ions close to the surface. N-doped electrodes have higher double layer capacitance, which means that there is a larger potential drop; Larger double layer capacitance means that more oppositely charged ions are kept within the double layer to counteract the electrostatic force from the electrode, and the increace of charge in the double layer effectively increases the potential drop.

Cola et. al. claims that a high concentration of Potassium ions would also give a high concentration of the redox couple, thus higher kinetics. However, an increase in the concentration of the redox-species, who are negatively charged will reduce the local charge of the electrolyte and in reality means a reduced potential drop and capacitance. There might be other mechanisms responsible for the increased kinetics.

For *Cola et. al.* the NCNT electrode showed fastest kinetics at 0.01 M, while at 0.1 M the performance of the NCNT electrode was reduced as the electron transfer became sluggish, such that the doping-free buckypaper showed faster kinetics. *Cola et. al.* assigned this effect to the strong compression of the double layer because of high concentration, and blocking of the surface by K^+.

The concenentration used in the experiment in this project is even higher (0.4 M), but still the NCNT shows better performance than all the CNT electrodes. To understand the catalytic effect of Nitrogen doping into CNT's it is important to understand the local structure and electron density on the CNT surface. The nature of the active sites coming from N-doping is still unclear, but the observations done so far can aid a fruitful discussion of the recation mechanisms taking place in the redox reaction occuring with the ferri/ferrocyanide ion.

Cola et. al. had incorporated approximatley 5 % Nitrogen, which is more than what was incorporated in the aligned tubes used here (1.5 %). The two most common binding modes for Nitrogen in CNT's when the doping is performed by plasma treatment of CNT's, as done by *Cola et. al.*, is the substitutional and pyridinic binding mode [42, 43, 20]. When N-doping is done in CVD, as here, pyridinic and pyrrolic binding modes are most common.

The binding modes are shown in figure 2.3. The pryidinic binding is sp^2 hybridization of N, bound to two C atoms and with a localized electron pair. The localized electron pair increases basicity, and are acitve in base catalyzed reactions. The pyridinic nitrogen contributes with electrons to the π-system, and makes the tube metallic. The substitutional Nitrogen contributes with 2 π-electrons. The pyrrolic binding mode is the sp^3 hybridization of N, which leads to structural

change and it is important for the bamboo structure observed in NCNT's. Typically, the bamboo structure have many edge defects and dangling bonds following with these.

The reaction mechanism of reduction and oxidation of Ferro/Ferricyanide is not known. What is known, is that Cyano-gruops can bind to the CNT [44]. It is also known that during catalysis of Ferrocyanide oxidation by some proteins, intermediate binding of the C≡N occurs[45]. Therefore it is here suggested that the electron transfer reaction of the Ferrocyanide complex involves intermediate binding of the Cyano-ligand with the CNT, and electron transfer to the iron. When one ligand is removed from the Iron complex, the positive iron will be exposed and seek towards areas with high electron densiy, *e.g.* the surface of the tube which has high electron density due to doping. A schematic figure of the proposed reaction mechanism is shown in figure 5.4. The Cyano-group can be adsorbed on the CNT, dangling bonds and pyridinic sites. It is believed that higher electron density enhances the binding of the Cyano-group. This indicates that the substutional binding mode also is very important for the reaction.

As N-doping increases reaction kinetics, it is suggested that N-doping increases the adsorbtion of C≡N. *Cola et. al.* had a higher level of Nitrogen than the NCNT's studied here. It might be that the reason for the slow reaction rate at high concentration is too strong adsorbtion of C≡N. Hence, there is a upper limit for N-doping, above which the ligands does not desorb and blocks the surface for reduction and oxidation.

Another reason might be that the increase in surface electron density will strengthen the adsorption of K^+ ions, so will the presence of pyridinic sites in analogy with the Li^+ ion[46]. The energy barrier for addition of one more potassium ion to the layer of ions strongly bound to the electrode surface (Helmholtz layer) will be smaller than the barrier of adding one more Cyano-group, as this involves dissociation of a rather stable iron complex to a less stable under coordinated complex. Energetically it is easier for K^+ to adsorb on a charged surface, and the adsorption depends on ϕ. The adsorption of Ferrocyanide includes partial dissocation of the complex, intermediate binding of C≡N and there can be electrostatic repulsion of the complex. The complex is also large and will have spatial requirements.

The effect of this will be a favourization of Potassium adsorption at the cost of Ferro/Ferricyanide adsorption at high levels of doping, and thus a reduction in reaction rate. The consequence of this is that there will be an ideal level of nitrogen doping for the catalysis of the current reaction.

The expermients in this project does not provide sufficient information to really establish the mechanism. Fore more insight, *e.g.* DFT caluclations can be done. However, by comparing *Cola et. al.* and this project, it seems as there is an ideal level of doping.

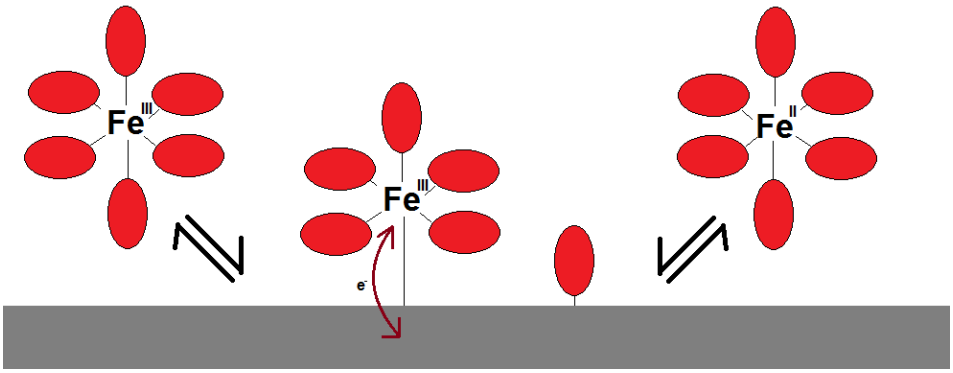

Figure 5.4: Simple schematic figure of the suggested reaction mechanism of Ferrocyanide reduction. A ligand is dissociated and adsorbed on the CNT. Iron is exposed and undergoes electron transfer. The complex is associated again.

Symmetry factor. As seen in figure 5.1 and 5.2, the peak currents for all the electrodes are symmetric around the same potential, indicating that the symmetry coefficient β is ca 0.5, and that the electrodes interact equally for both reduction and oxidation. This means that the electrodes have the same catalytic effect as anode and cathode and a symmetric electrode set-up can be used in an actual thermocell. *Cola et. al.* also found that the symmetry factor of CNT and NCNT electrodes was ca 0.5.

Effect of CNT length on E_p. The displacement of E_p increases with increasing CNT tube lenght. Tubes synthesized in similar fashion should have similar quality and therefore the tube surface has similar behaviuor towards the catalysis of the redox reaction. The shift in E_p is due to slower charge transfer, but the sluggishness of the charge trasfer cannot bue due to the tube quality. It is seen in figure 5.1 a) that the 110 μm tubes have reversible charge trasfer at scan rate v = 0.01 V/s, but at higher scan rates it becomes sluggish (v=0.1 V/s). The voltage employed on an electrode effectively catalyzes a reaction as energy of the species Ox, in Ox + $ne^- \rightleftharpoons$ R, is increased with nFE, E is the potential. The transition state itself increases with βnFE. Hence the redction of the energy barrier is proportional with (β-1)E.

It is here assumed symmetic charge transfer, and $\beta = 0.5$. When the voltage is changed as follows,

$$\frac{dE}{dt} = v$$

The barrier changes at a rate

$$\frac{dE_a}{dt} = -nF(1-\beta)v$$

The reaction rate follows an Arrhenius behaviour. By derivating the rate constant k with respect to time it is found that the reaction rate increases exponentially with E, and proportinal to v.

$$\frac{dk}{dt} \propto e^{(1-\beta)nFE(t)/RT}v$$

This derivation is shown in Appendix C. For slow scan rates, the change in reaction rate will be much slower than the change in reaction rate for fast scan rates. This also means that the current and change in current with time is less. For a high change in current, the diffusion of species must respond to proportionally to keep up the elecron transfer rate. However, diffusion to the roots of the carbon nanotubes when the tubes are long can be hindered.

A dense network of cabron nanotubes can be as a porous material, if the mean free path of the ions is comparable to the "pore" size[40]. The denser the tubes, the slower is diffusion. The consequence is that the concentration of the electrolyte close to the roots is low, and hence slower reaction.

I_p magnitude. I_p for the two NCNT samples differ. It is known that the samples can be non-uniform. At different parts of the sample, the difference in length can be easily be $\pm$ 500 nm. When the tubes are as short as 1-2μm, these non-uniformities will greatly affect the observed current. By knowing the tube lengths are within 1.7 $\pm$ 500 nm, the specific surface area can differ with 50 %. Current scales proportianlly with surface area A, and it is seen that the absolute magnitude for the second NCNT sample is 0.032, while 0.020 for the first. The difference is clearly due to non-uniformity and hence differnece in A.

The normalized current decreases with tube length. This is due to the sluggishness of the electron transfer due to slow diffusion within the tubes, observed by E_p-displacement. Due to sluggish electron transfer, there will be an optimim tube lenght for the electrode for maximum reaction rate. Longer tubes gives a higher surface area, so there will be a competition between sluggish-ness and surface area. Which length will maximize the current?

An interetsing study that can be done is to investigate current as a function of tube length. Above a certain length diffusion will start to be the limiting factor for the reaction. This tube length can be found by investigating the current density, *e.g.* the normalized current, and see when the normalized current starts to drop significantly. Figure 5.5 shows the magnitude of the peak current in CV normalized with respect to length. It is seen that the increase in current from 14 to 5 μm is much higher than the increase from 50 to 14 μm. This indicates that already at 14 μm, there are concentration gradients along the tube. For a less dense network, diffusion will not be limited and the ideal electrode material as aligned, but not

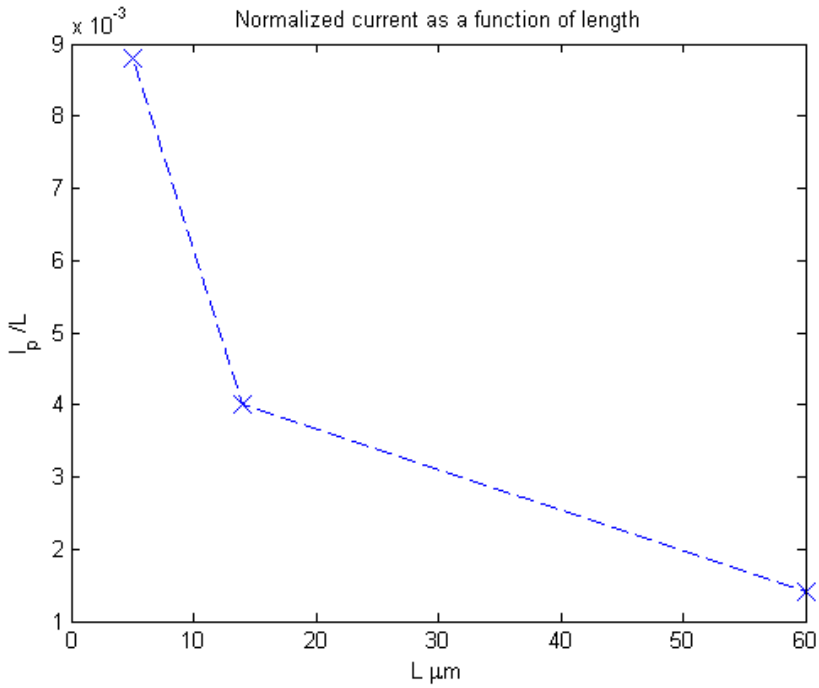

Figure 5.5: Peak current in CV normalized with respect to tube length, as a function of length. v=0.1 V/s, 0.4M

densely aligned tubes. This is a difficult balance, as alignment is a direct effect of density.

Cyclic Voltammetry with TBAN

Due to adsorption of TBAN on the electrodes, Cyclic Voltammetry in this electrolyte will give rise to artifacts [47], and the method cannot readily be used to compare reaction kinetics of different electrodes.

5.2 Cell performance

The performance of electrodes and electrolytes was tested by measuring V_{oc} and I_{sc}. TBAN and Ferri/Ferrocyanide was tested as electrolytes with CNT (50 μm) or NCNT (1.7 μm) as electrodes. The electrodes were kept in a vertical position.

Thermocell orientation

The electrodes in the thermocell can be horizontal, with the hot electrode above the cold electrode or the cold electrode above the hot electrode. The electrodes can also be vertical. *Baughman et. al.* [3] investigated these three orientations. The hot above cold configuration is the least efficient. As heat transport in an aqueous liquid is mainly by convection, *e.g.* hot liquid flows up, this configuration will have the highest thermal resistance as the heat transfer through the electrolyte will be only by conduction. The convective transport will not contribute to heat transport as the fluid is heated from the top.

The drawback with this configuration is that the redox products at the anode will be transported to the cold cathode only by diffusion due to concentration gradients. At the cold electrode the product is also accumulated as it will be prohibted from flowing to the hot electrode due to lower thermal energy. The absence of effective mixing will reduce the current as the concentration at each electrode will be that of the equilibrium. This will reduce the overall efficiency of the device.

When the hot electrode is below the cold electrode, the conductive heat transfer will increase the mixing, and the current is kept high. The products if the hot electrode is readily trasported away, to the cold electrode due to bouyancy. Thermal resistance will be less in this configuration as both conductive and convective heat transfer occurs.

It was found by *Baughman et. al.* that the vertical setup gave the same currents as the hot below cold conficuration. The electrical resistance in the solution was more stable for the verical setup than for the horizontal setup. Therefore, this setup is used in this project.

In the vertical setup, both convective and conductive heat transfer occurs, but is directions normal to eachother. This gives a more complicated temperature profile,as the liquid at each electrode may have different temperatures, depending on it's z-coordinate.

5.2.1 Electrolyte testing

Ferro/Ferricyaide

0.4 M equimolar $K_3Fe(CN)_6/K_4Fe(CN)_6$ was solvated in De-ionized water. 50 μm long ACNT's and 1.7 μm long N-CNT's on aluminum foil was used as electrodes. The electrode area was 7.06 cm^2 and electrode separation 2.2 cm. V_{oc} and I_{sc} was measured with a mulitmeter. The results are shown in table 5.3.

Open circuit voltage. The theoretical value of the Seebeck coefficient is $\approx$ 1.43 mV/K. Most of the measuerd data lies close to this, +/- 0.3 mV/K. Deviating from this value, is the N-CNT(hot)-CNT(cold) configuration, where the Seebeck coefficient is 1.0 and 0.8, for the temperature gradients 61 and 41 K respectively.

Hot	Cold	T_c	T_h	dT	V_{oc} [mV]	S_e [mV/K]	I_{sc} [μA]
N-CNT	N-CNT	29	57	28	52	1.8	240
N-CNT	N-CNT	44	84	40	48	1.2	430
CNT	N-CNT	27	61	34	51	1.5	126
CNT	N-CNT	38	85	47	75	1.6	250
N-CNT	CNT	18	59	41	40	1.0	33
N-CNT	CNT	27	88	61	50	0.8	50
CNT	CNT	21	56	35	52	1.5	60
CNT	CNT	46	84	38	140	3.7	190

Table 5.3: Measurement of I_{sc} and V_{oc} for a thermoelectric cell with 0.4 M Ferrocyanide/Ferricyanide. T_h is the temperature at the hot electrode. T_c is the temperature at the cold electrode.

Also, the CNT-CNT configuration for the higher temperature (46-84^{o}C) has a measured Seebeck coefficient much higher than the theoretical, it is 3.7 mV/K.

+/- 0.3 mV/K is not necessarily a large deviation. The temperature measurement contributes to some error. One of the thermocouples used is a thermocouple calibrated for high temperature measurements, and this deviated some from the real temperature. Saying that the error in temperature measurement can be in average 2 degrees for each electrode, some of the deviation is covered for. A second contribution is the thermal convection of water, warm fluids flows up and cold fluid sinks down. To avoid water leakage from the cooling compartment, the flow with cooling water had to be kept low and the compartment did not fill up. Only half of the aluminum plate was cooled effectively, such that the electrolyte at the top could have been warmer than at the bootom. The voltage produced by the cell would be reasonably that representing the average electrode temperature as the chemical potentials would even out. Hence, the measured temperature difference *can* have been less than the real temperature difference (and S_e higher). The magnitude of this would depend on the history of the device and the actual flow of cold water, which was varied.

A third, but very important factor, that adds to the error in measurement is the risk for current leakage. The termocell was held together by steel screws, which are highly conductive. The screws was taped with electrically insulating tape to insulate them from the electrodes. To ensure sufficient insulation the resistance between the screws and the aluminum plates was measured. The resistance was 1MΩ, and it was assumed that the leakage of current was neglectible. However, during an open circuit measurement the resistance of the multimeter is also great and there can be small current leakage leading to a lower measured voltage.

Especially for the measurement of NCNT(hot)-CNT(cold), where the Seebeck coefficients are low, leakage can have been the problem. The resistance was controlled for the reverse set-up (CNT on the hot side), and was slightly less than 1MΩ. To swap the electrode setup, the tubes with cooling water was coupled to the previous hot compartment and the tubes with hot water was coupled to the cold

compartment. The resistance was not controlled after this manouver, but it might be that the tape and glue that had been cold and suddenly rose 40-60 degrees in temperature softened,meaning that the electrical contact between the electrode and screw had less resistance. Also, now the thermocouple with the largest error was placed on the opposite side, compared to all other measurements. This means that the error that was fairly systematic for all other measurements changed.

The third offset S_e value is the symmertic CNT-CNT system at $T_{avg} = 65\ ^oC$. S_e was calculated to be 3.7 mV/K. Either the cell must be far from equilibrium, or there are som impurities giving leading to offset values. The aluminum support plates are not electrically insulated from the water cooling and heating system. There might also have been reactions with impurities in the water. This can give rise to both too high or to low values for both V and I, depending on the nature of the reactions.

Regarding measurement of short circuit current the resistance of the mulitmeter will be very small, rendering the current measurements relatively reliable as the current passing though the multimeter would be 10^6 higher than the leakage.

Short circuit current. As discussed above, the problem of leakage is not such a big problem for short circuit measurements than for open circuit measurements, as the multimeter resistance is much lower than the resistance in the path of leakage. The measured short circuit current for different electrode configurations vs average temperature is shown in figure 5.6. The NCNT-NCNT symmetric configuration has the highest short circuit current: 240 μA (T_{avg}=43^{o}C) and 430 μA (T_{avg}=64^{o}C). The NCNT(cold)-CNT(hot) has the second highest short circuit current, ca 45 % less than the symmetric NCNT configuration. The reverse configuration, CNT(cold)-NCNT(hot) has the poorest current density, and the current does not show not show significant increase with temperature.

The symmetric CNT-CNT configuration shows a current that is 75 % less than the NCNT-NCNT current, 60 μA, and then a great increase of current to 190 μA for the higher average temperature, 55 % less than what the nitrogen doped electrodes show.

The superior performance of the Nitrogen doped electrodes confirms what was concluded in the previous section: N-CNT's have higher reaction kinetics than CNT's. Despite that the ACNT electrode have higher surface area, the total current delivered is less. In the CV experiments it was found that long tubes had a sluggish electron transfer due to lower diffusion to the roots of the nanotubes. For a thermocell in operatrion, the poor diffusion leads lower concentration amoung the tubes, and accumulation of redox products. The reaction will stop when the equilibrium concentrations have been reached. Only the part of the tube where species can readily diffuse to or from will contribute to current.

Which reaction is rate limiting? In the thermocell, the anode is the warm electrode and cathode is the cold:

Cold electrode, cathode

$$Fe^{3+} + e^- \rightarrow Fe^{2+}$$

Hot electrode, anode

$$Fe^{2+} \rightarrow Fe^{3+} + e^-$$

As discussed in the previous section, the symmetry coefficient β of the electrodes is ca 0.5, in agreement with [13]. Hence, under same conditions the reaction rate of the reduction and oxidation will be similar. But the ions at the cold electrode have less thermal energy than the ions at the hot electrode, and then slower kinetics accordinig to the Arrhenius equation, see section 2.6. The cold electrode might also have a higher concentration of ions because of the Soret effect. This will increase the kinetics unless there is competetive adsoprtion from Potiassium and more sluggish electrontransfer.

By comparing the CNT(hot)-NCNT(cold) set-up with the symmetric CNT setup, it is seen that the current increases when the cold CNT cathode is replaced by an NCNT electrode. This means that for the symmetric CNT case, the cold CNT cathode is the current limiting electrode. When also the CNT hot anode is replaced by NCNT, giving symmetric NCNT setup, the current is even higher, which means that the hot CNT electrode is current limiting for the CNT(hot)-NCNT(cold).

It is possible to deduce some information about the catalyitic effect of NCNT vs CNT's from this, using the following observations: When $T_{avg} = 63$ ^{o}C for the CNT(hot)-NCNT(cold) setup, the current delivered is similar to the current from the symmetric NCNT set-up with $T_{avg} = 43$ ^{o}C. The hot CNT elecrode is rate limiting, and has T = 85 ^{o}C. Now we are assuming that the cold NCNT electrode is rate limiting in the symmetric case due to lower thermal energy, it has T = 29 ^{o}C. When also assuming that the CNT(hot) is reaction rate limited (not diffusion limited), the rate constants are equal for these two different temperatures. By using the Arrhenius equation, it can be calculated that $E_{a,CNT} = 1.2$ $E_{a,NCNT}$.

The assumption that the long tubes are reaction rate limited is only partially true, as there might be diffusion restrictions due to the long tube lengths. The contribution to the activation energy found above is not only the activation energy of the reaction, but also the energy barrier of the sluggish diffusion to the electrode.

By comparing the symmetric CNT set-up with the CNT(cold)-NCNT(hot) set-up it would be expected that these would deliver similar currents when knowing that the CNT electrode is rate limiting. This almost true when T_{avg} is 38 ^{o}C, but not true for the higher temperature. As the Seebeck coefficient calculated for the CNT(cold)-NCNT(hot) setup was quite off, there might have been reasonable current leakage. This also explains the small difference for the lower temperature. The results for the CNT(cold)-NCNT(hot) set-up is therefore disregarded.

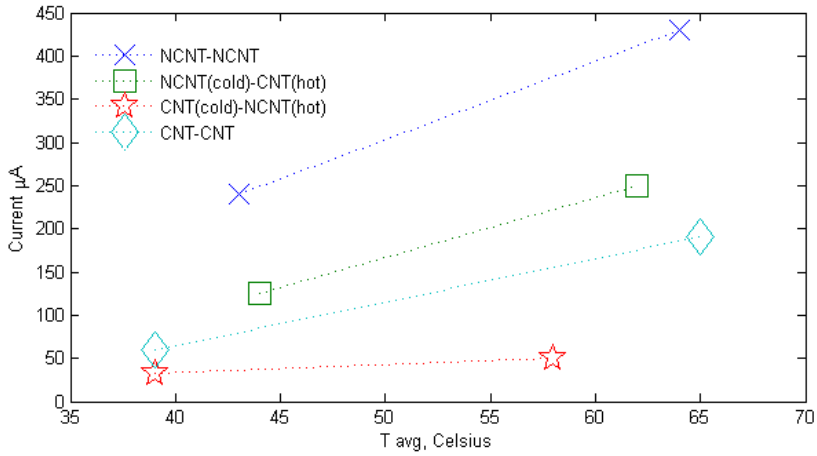

Figure 5.6: Short circuit current for different electrode configurations as a function of average temperature. 0.4 M Ferri/Ferrocyanide. The dashed lines are guides to the eye.

Figure 5.6 shows the important trends. The symmetric NCNT-NCNT setup has the best performance, due the faster charge transfer characteristics shown in the previous section.

TBAN

Open circuit voltage. A thermoelectric cell containing 0.1 M TBAN electrolyte in dodecanol was held at stable electrode temperatures ($T_h \approx 57^oC, T_l \approx 25^oC, +/-2^o$). The development of S_e as a function of time is shown in figure 5.7(top panel). After nearly 2 hours, the value had stabilized around 6.5 mV/K. This is somewhat less than the value found by Guenon et al.[12]. As discussed in the above section regarding ferrocyanide, a small leakage of current can explain a lower value. Also, it was observed that the solvent adsorbed into the carbon tape. This will increase the resistance, leading to a voltage drop between the electrodes and multimeter. TBAN is slightly hydroscopic, and small amounts of water is soluble in dodecanol. The experiments was performed in ambient atmosphere, such that some water can have been adsorbed. Presence of water will reduce the Eastman entropy of transfer, as the structure making effect of the TBAN molecule will be reduced; The structure making effect comes from the preferential orentation of the polar OH-group of the alcohol towards the TBAN cation. As the alcohol is long-chained there is a high entropy change related to this bonding. The small polar watermolecule will hydrate the cation, and the entropy assosciated to these bonds are much less. A reduction of the Seebeck coefficient will be the result of this.

The solidification temperature of dodecanol is 24^oC. This may reduce the applicabilty of this electrolye, as temperature restrictions must be employed to keep the electrolyte in liquid phase. During one experiemt, the temperature at the cold electrode was kept too low, such that some of the electrolyte became solid on the electrode. Figure 5.7 shows the development of the Seebeck coefficient for this system. The Seebeck coefficient stabilized around 11.5 mV/K, nearly the double of the system where the electrolyte was fully in liquid phase. As a solid, the electrolyte is ordered and transport of one ion from solid to liquid involved a large change in entropy. It will be interesting to evaluate the potential of a system when the electrolyte is partially solid. It would be expected that the current would be reduced, as the ions in the solid phase will have much lower mobility then those in the liquid phase. There is a class of electrolytes called "gel electrolytes", a swollen polymer network consisting en electrolyte. These are often used in batteries. Their conductivities are much better than the conductivity of TBAN in dodecanol [12, 48]. The polymer network can be engineered such that the molecular interactions at the electrodes are different such that the system exhibits Seebeck effect caused by entropy of transfer. Very interesting is the research paper by Brown et. al [6], investigating thermoelectricity in natural and synthetic hydrogels. The sensory system of some animals is very sensetive to electrical fields and temperatre, and exhibit a natural Seebeck effect. ZT, figure of merit for natural shark gel is 3 times ZT for 0.1 M TBAN in dodecanol.

Short circuit current. The short circuit current of the TBAN thermocell was measured. The inital current for both CNT and NCNT electrodes was 13 and 13.5 μA, while it decreased to less than 1 μA in some seconds. A second current measurement was done ca 1 hour later. The second mesurements had initial currents lower than the first measurement, around 6 and 8 μA. In figure 5.8 the current is shown as a function of time for two different electrode set-ups: Symmetric CNT electrodes and symmetric NCNT electrodes. The concentration of TBAN in dodecanol is 0.1 M for all measurements except for CNT 2nd measurement where it is 0.2 M.

What is seen in this figure is that the initial currents for the first measurements is 13 (CNT) and 13.5 (NCNT) μA, and the decrease in current for the NCNT electrode is faster than for the CNT electrodes. By normalizing the inital current with respect to length it is seen that the normalized current for NCNT is 37 times higher than the current of the CNT electrode. The kinetics of the NCNT electrode must be faster.

The second measurements has lower initial currents. The rate of decrease is similar for the two measurements with NCNT electrodes. The two measurements of the CNT electrodes is done with different concentration and comparision should be done carefully. However, the rate of decrease is less for the CNT electrodes than the NCNT electrode. After a while the current when using N-CNT electrodes had decreased to a stable value of 0.1 μA and 0.4 μA for CNT electrodes.

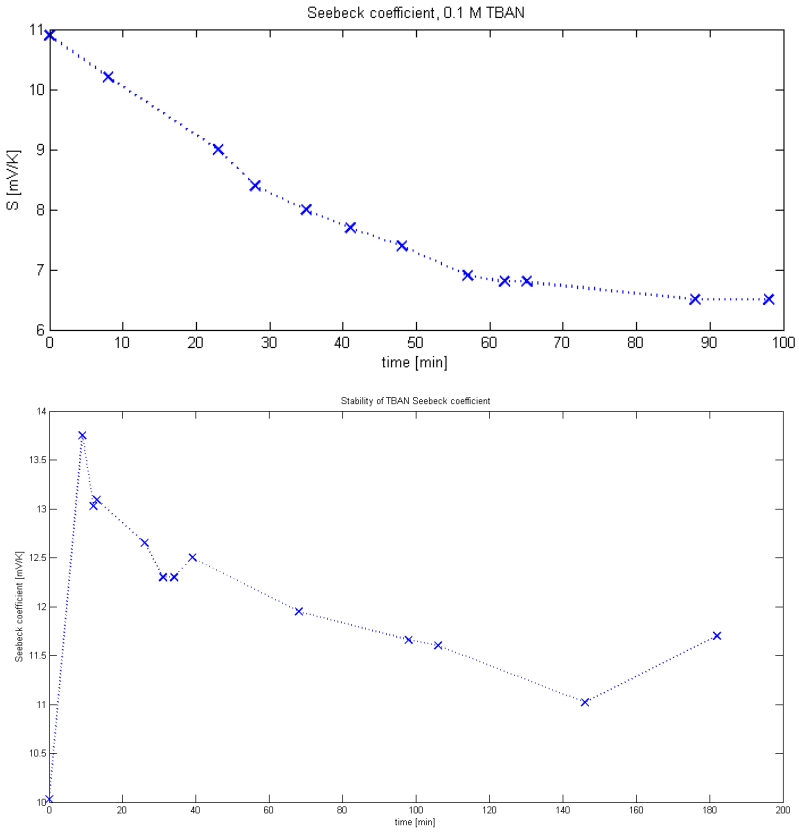

Figure 5.7: A thermoelectric cell held at stable temperatures over time. 0.1 M TBAN in dodecanol and CNT electrodes.

By viewing the graph, it seems as an exponential decay. Such a decay is described by the formula below, where I is current, t is time, I_0 is the initial current and α a constant. The practical intepretation of α is that it determines the the "strength" of the declination, the driving force for reducing the current, e.g. the rate of catalyst poisoning. The reduction in current can be due to blocking of active sites. If α is constant, the probablity of inhibitative adsorption is constant.

$$I(t) = I_0 e^{-\alpha t} \Rightarrow lnI(t) = lnI_0 - \alpha t \tag{5.2}$$

Plotting the logarithm of I versus time should give a linear function where the slope is α. This plot is found in figure 5.9. The slope is initially linar, but changes after some time. The slope of the NCNT electrode is steeper, indicating that "catalyst poisioning" of NCNT is faster than on CNT's. We need two know what can happen on the surface.

The current must have it's origin in some reduction and oxidation reaction. Rightmire et al [49] suggests two mechanisms for oxidation of alcohol into aldehyde on Pt electrodes: By adsorption of a C-atom to the catalyst or adsoprtion of an O-atom. Reduction can occur via reduction of nitrate[50]. The TBAN cation is not likely to be involved in the redox process, the hydrocarbon bonds are strong and the N-atom is sp^3 hybridized, all valence electrons contributes in bonding. Oxidation would indicate removal of 1s electrons, which are strongly bound to the nucleii.

Adsorption of C on Pt, fast

$$RCH_2OH \rightleftharpoons R\dot{C}HOH + H^+ + e^- \tag{5.3}$$

Reaction into aldehyde, slow

$$R\dot{C}HOH \rightleftharpoons RCHO + H^+ + e^- \tag{5.4}$$

Adsorption of O on Pt, slow

$$RCH_2OH \rightleftharpoons RCH_2\dot{O} + H^+ + e^- \tag{5.5}$$

Reaction into aldehyde

$$RCH_2\dot{O} \rightleftharpoons RCHO + H^+ + e^- \tag{5.6}$$

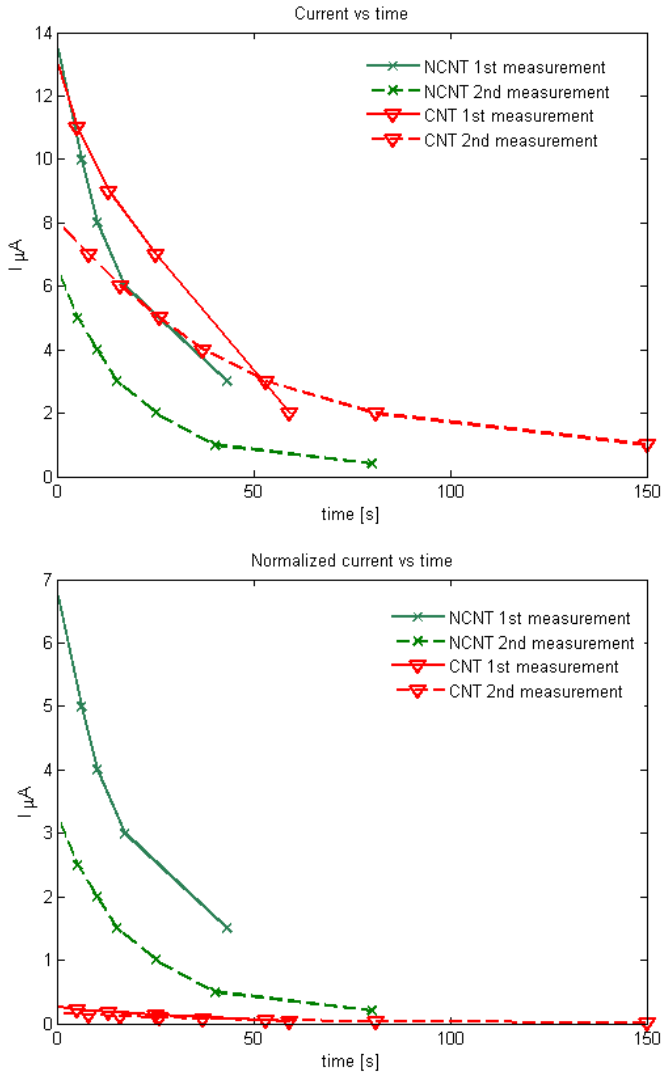

Figure 5.8: Manual recording of current as a function of time for aligned CNT and NCNT electrodes in 0.1 or 0.2 M TBAN-dodecanol electrolyte. Average temperature: 44 (NCNT) and 40^o C(CNT). The first measurement is the very first measurement of the short circuit current, the second measurement is a new measurement done 1 hour later. The concentration for the NCNT electrode and the first measurement with CNT electrodes is 0.1 M, and 0.2 M for the second measurement with CNT's. Top panel: Current. Bottom panel: Current normalized with respect to length.

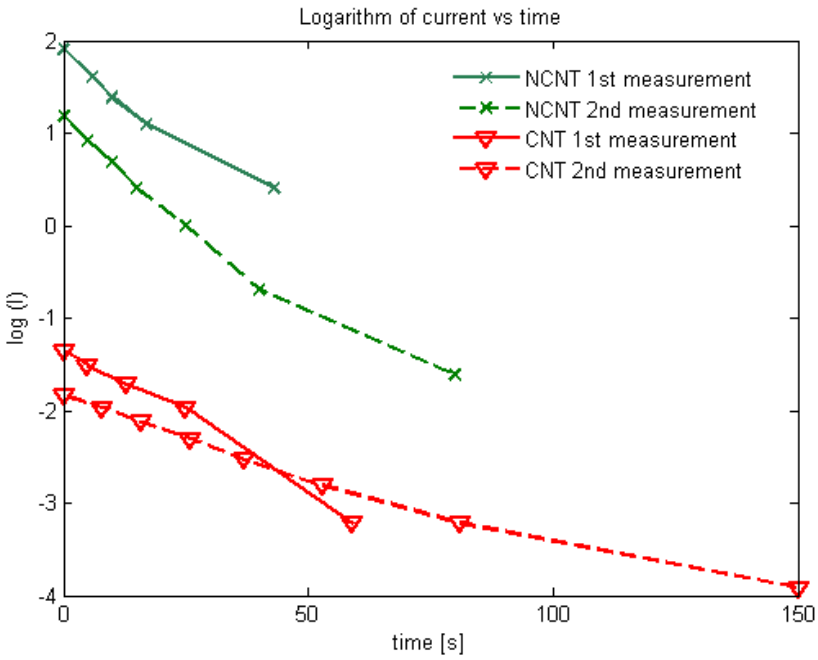

Figure 5.9: Natural logarithm of I_{sc} vs time, for a TBAN thermoelectric cell with symmetric electrodes of aligned CNT's or N-CNT's. I is normalized with respect to tube length

The half cell reaction

$$RCH_2OH \rightleftharpoons HOCH_2R + 2H^+ + 2e^- \tag{5.7}$$

Nitrate reduction.

$$NO_3^- + 2H^+ + 2e^- \rightleftharpoons NO_2^- + H_2O \tag{5.8}$$

Total reaction

$$RCH_2OH + NO_3^- \rightleftharpoons RCHO + NO_2^- + H_2O \tag{5.9}$$

The Nitrate reduction mechanism on carbon nanotubes is not known. Studies on Nitrate reduction ot Pt suggests that the adsorption of the Nitrate ion is not sensetive to the strucutre on single crystalline Pt, but the reaction is sensetive to impurities[51], and that adsorption of the nitrite is rate limiting[50]. Carbon is electron accepting, the negatively charged nitrate can adsorb on the CNT surface, and interact with dangeling bonds. The reaction as written above requires contribution of a proton. Alcohol can deprotonate and their pKa's are around 2.5, meaning that there can be a substansial amount of protons in the solution. Deprotonation is a base catalyzed reaction. Presence of pyridinic Nitrogen from nitrogen doping can facilitate the deprotonation of alcohol at the cathode and supply protons to the Nitrate reduction. It can then be assumed that it is beneficial for Nitrate to adsorb in the vicinity of pyridinic Nitrogen. Deprotonation is as follows:

$$R - OH \xrightarrow{N-pyridinic} RO^- + H^+$$

The deprotonated species does not need to desorb from the pyridinic site.

It is accepted that the oxidation of allyl alcohols goes via an adsorption step, and that the catalysis by metals as Pt and Ni is much more efficient than the catalysis by carbon itself. Therefore litterature today studying the catalysis of alcohol oxidation is focused on the use of CNT's as support for noble metals as the above [52]. The adsorption on pristine CNT's are limitied. Alcohol oxidation can be a base catalyzed reaction. Adsorption of the O-atom on pyridinic N can be an important reaction route. Or adsorption of alcohol O or C-atoms on dangeling bonds assoscated with defects can be important. The rate of reaction 5.5 is assumed to be fast, it is the adsorption of the alcohol is rate limiting. The presence of pyridinic N and defects coming from Nirogen doping enhances dodecanol adsorption and oxidation compared to pristine CNT's. The adsorbed alcohol does not need to desorb, meaning that the reaction stops after step (5.3).

The adsorption and redox reaction of both species is difficult. This is also reflected in the very low current delivered by the cell.

It is known that TBA can adsorb to an electrode surface and has slow desorption kinetics[47, 25]. The adsorption of TBA is promoted by high electron density at the surface as it has positive charge. When current is drawn from the thermocell, the cathode will have increased surface charge. Clearly there might be a competetive adsorption between TBA and Nitrate. It can be assumed that TBA has higher adsorption kinetics and will block the Nitrate sites, as it is belived that the adsorption kinetics of Nitrate is slow. Hence, it can be argued that adsorption of TBA inhibits reduction of nitrate. When the circuit is opened the TBA molecules will desorb. This is also seen, as the inital currents for the second measurements is higher that the terminal currents of the first measurements. However, desorption is slow and seemingly it will take more than 1 hour for all TBA to desorb.

It would be expected that if TBA was the dominating adsorbing species, higher concentration of TBA would give a more rapid fall in current, this is not the case. It was seen that the slope for the second discharge when using 0.2 M TBAN was less steep compared to the 1st discharge of the 0.1 M test with the CNT electrode. As the 1st and 2nd discharge for the NCNT electrode has initially similar slopes it would be assumed that the initial slope is independent of wether it is the first or second discharge.

A third reason can be the effects of the water product. For each 2 electrons, a water molecule is formed. Water has limited solubility in dodecanol, which means that a thin layer of water is formed at the electrode. This can hydrate the Nitrate, such that the activity of the Nitrate is lowered, and reduction ceases. For the 0.2 M solution, the decrease is less rapid as the concentration of Nitrate is twice as large compared to the other experiments. The higher concentration of Nitrate gives a higher activity and hence less rapid decrease in current. Also, as TBA is a surfactant it will go to the dodecanol-water interface. This might block for transfer of Nitrate to the electrode surface and trasport of the Nitrite product away from the electrode.

In the logarithmic plot, it is seen that α is not constant, but there are two regimes. The inital seconds, when 1st and 2nd "discharge" of an elecrode have similar slopes. Later, the slope is reduced, and this slope varied for all samples and discharges. The presence of 2 "regimes" might indicate that there are several contributing factors, and different factors dominate the initial and later stages. The slope of the NCNT electodes is at all times steeper than that of the CNT electrode. This can be due to the much higher current density. All these observations are interesting, but needs further research. Studies of the activity of Nitrate in water versus the activity in dodecanol, and the effect of the water product is interesting.

What can be concluded, is that NCNT electrodes have the fastest kinetics, but the electrolyte is not interesting for applications due to low conductivity and current declination during operation.

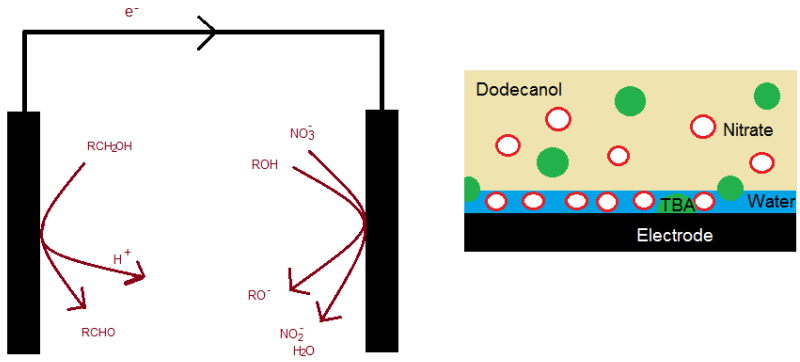

Figure 5.10: Anode and cathode reactions, and the formation of a thin water layer on the electrode as the reaction goes on, solvating Nitrate and reducing Nitrate activity, and the formation of a surfactant layer.

Electrolyte	T_{avg}	dT	η	η of carnot	P
Ferrocyanide	43	28	0.0006 %	0.007 %	3.13μW
Ferrocyanide	64	40	0.0007 %	0.006 %	5.00μW
TBAN	41	32	0.0005 %	0.004 %	0.65μW
Baughman	55	30	0.0235 %	0.269 %	105.75μW*

Table 5.4: Summary of efficiencies η and power for the thermocell in this paper, compared to a thermocell developed by Baughman et al[9]. *Power for an electrode with electrode area similar to the the electrodes in this project.

5.3 Thermocell performance

Table 5.4 summarizes the maximum power (P_{max}=$V_{oc}I_{sc}/4$), thermocell efficiencies and efficiencies relative to the Carnot efficiency for the NCNT-NCNT Ferro/ Ferricyanide and TBAN-cell. For comparision, a thermocell created by Baughman et al. is included in the table. This thermocell used buckypaper electrodes with 2.6 cm separation, and vertical electrode setup. The thermal resistivity of the Ferrocyanide electrolyte is assumed to be similar to the thermal resisivity of water. Regarding the short circuit current for TBAN, the maximum initial current is used. Overall, the efficiencies are very low.

The efficiency of the TBAN-cell is 0.004 % which is somewhat lower than the Ferrocyanide-cell (0.007%) at comparable temperatures. The efficiency is proportional to the current density, thermal resistance and S_e, as shown in formula 2.1. While the TBAN current is 18 times less than the Ferrocyanide current, the voltage is 4 times higher and the thermal resistivity is nearly 4 times higher. These

partially compensate for the loss in current. The power delivered by the TBAN-cell is 5 times less than the power delivered by the Ferrocyanide-cell, as the gain in voltage does not compensate for the reduced current.

Because of the declination in current discussed in the previous section, TBAN is not suitable as electrolyte. The long term current approaches zero, and the cell is not applicable. However, it should be possible to find other organic or gel electrolytes with high S_e where adsorption is not as problematic. In addition to higher voltage, these electrolytes often have higher thermal resisitvities than water such that the electrode separation can be smaller than the separation in an aqueous cell. By reducing the electrode separation the electical resistance across the cell is reduced. This increases the current.

Let's say there is an electrolyte for which stability is not a problem, with S_e similar to S_e for TBAN in dodecanol, and a solvent with similar heat resistivity as dodecanol. By reducing the electrode separation to 5 mm, the electrical resistance will reduce to ca 1/4. This increases the ionic current times 4. Assuming also that suitable electrode functionalization would improve reaction kinetics, currents similar to the ferrocyanide-cell can be obtained. It will be important that the electrolyte causing the Seebeck effect also is the red-ox active species. Regarding the quaternary amine, it is not likely for this to be oxidized to a 2+ state as this would mean removal of 1s electrons since all 2s and 2p electrons contribute in bonding. However, the amine can be functionalized with different side groups that are redox active. The redox reaction should avoid to have water as a product. To investigate metallorganic species, where a metal ion coordinated by organic groups can be reduced and oxidized is interesting for futrure work.

Sadly, it is seen that the efficiencies obtained in this project is nearly 40 times less than the efficiencies obtained by Baughman et al. Baughman et al claims to have achieved 1.4 % efficiency relative to the Carnot efficiency. After careful study of the results presented in paper [9], it was discovered that this efficiency is calculated by using the optimal results from different expermiments. The efficiency obtained in the current project should be compared to the efficiency of an experiment with similar set-up and temperatures. In an experiment using 30μm thick MWNT buckypaper electrodes with 2.6 cm separation, the efficiency was only 0.269 %. The respective current density was 15 A/m^2. The highest current density achieved this diploma work was 0.6 A/m^2, 25 times less. The average temperature was 55 and 64 degrees C, respectively. The thermal energy in the current cell was higher than in the cell of Baughman, and the current should have been higher.

The Baughman electrode is 30μm, 18 times thicker that the the NCNT electrode. As the electrode separation is larger also, the efficienies should be normalized with respect to electrode thickness and electrode separation. The calculations are shown in the appendix D. The resulting normalized efficiecy relative to the carnot efficiency show that $\eta_{Baughman} = 2.14\eta_{NCNT}$. As the numbers are normalized, the difference in efficiency comes from difference in reaction kinetics, electrode

resistance and other sources of error.

There are several sources of error associated with the test cell used in this project, especially important is systematic leakage of current due too insufficient insulation of the electrode support plates. The errors are fairly systematic for this project such that the electrodes and electrolytes can be compared within this project, but not with other projects.

For future work a better test cell system should be designed.

Still, the most interesting direction is to find better electrolytes with high S_e. Fundamentally, efficiencies of a thermocell using aqueous electrolytes is limited and efficiencies much above 1.5 % will be difficult to achieve as water molecules contribute much to thermal transport but not to ionic current.

Chapter 6

Conclusion

This chapter summarizes the main findings in this project.

6.1 Growth of Aligned CNT's and NCNT's

Aligned and uniform CNT's on Aluminum foil was synthesized by CVD using a pre-deposited 2 nm layer of iron catalyst. The CVD gas composition was 160 mL/min Ar, 7 mL/min H_2 and 20 mL/min C_2H_4. Tubes were grown at T_{wall} = 640, 650 and 660 ^oC. The fastest growth kinetics was at T_{wall} = 660 ^oC. After 2 hours growth tubes up to 110 μm was grown. The diameters were 15 nm.

Due to rapid catalyst poisioning, it was found necessary to anneal the samples in an NH_3 containing atmosphere before CVD. Anneling forms Iron Nitride, a catalyst that has lower activity and longer lifetime than Iron. The duration of annealing showed to affect alignment and tube length. Samples annealed for 10 minutes was shorter and exhibited more curling than samples annealed for 30 minutes. A possible reason is non-uniform particles leading to different growth rates, poorer alignment and curling. Curling hampers diffusion of gas species to the catalyst, giving slower growth rates. Ammonia can function as an etching agent, such that smaller and more uniform catalyst particles are formed. Hence, the unifromity of the catalyst after 30 minutes annealing is better than after 10 minutes, where 30 minutes annealing is yielding long and aligned tubes.

It was also found that a too high partial pressure of H_2 (H_2:Ethene=1:1) leads to competetive adsorption og Hydrogen and reduced CNT formation as H_2 effectively reacts with dissociated carbon.

N-doped aligned CNT's were grown by the floating catalyst method, at 640^oC. 0.05 M ferrocene in ethanol was injected 20 mL/min, using Ar, NH_3 and H_2 as carrier gases. Ca 1.5 % Nitrogen was incorporated and the pyridinic binding mode was dominating. Increasing the partial pressure of ammonia lead to higher N-

incorporation, but also a decrease in reaction rate and less uniformity. At x(NH_3) = 0.35, the tubes were fairly uniform and 1% N was incorporated. At x(NH_3) = 0.9 the tubes was non-uniform and 1.5% N was incorporated. The method was not optimized. Attempts to optimize the method should consider to reduce the injection rate of the floating catalyst and the total carrier gas volume.

6.2 Thermoelectric performance

Ferro/Ferricyandie was more efficient than TBAN as electrolyte. The highest efficiency for the Ferro/Ferricyanide based cell was achieved with aligned NCNT electrodes. The efficiency of this setup was 0.007 % of the Carnot efficiency. When normalizing the efficiency with respect to thermal resistance and tube length, it is seen that the efficiency is approximately half of the efficiency achieved for a similar set-up by Baughman et. al.[9]. Important reasons for the difference in efficiency are current leakages in the test cell.

In CV, NCNT electrodes showed to have faster reaction kinetics than CNT electrodes, even at high concentrations. Regarding the mechanism of reduction and oxidation of the Iron Cyanide complex, it is suggested that it involves an intermediate binding of a Cyano-ligand. N-doping imporves this binding, but too high doping gives too strong C≡N adsorption, or inhibitive adsorption of potassium, resulting in lower current. To establish the correct mechanisms, DFT calculations can be done. Qualitatively, it was found that there will be an optimal level of doping for which the reaction rate is maximized.

The performance of the electrodes was reduced with increasing tube length as diffusion into the void between the tubes is slow and there will be low concentration closer to the roots of the tubes.

TBAN in dodecanol was found to be problematic as electrolyte, as it did not show stable current, but a rapid decrease in current. The reasons for this is not clear but possible problematic aspects are the adsorption of TBA and that water is one of the redaction products, and the hydration of Nitrate reduces the activity of the reduction reaction. Several possible reasons have been discussed, but no conclusions can be made from the data of this project. Despite high voltages in the TBAN-cell, the current and conductivity was very low, the current approached zero with time.

Still, the most interesting direction of research is the organic electrolyte path, as water based thermocell have an upper limit of performance as water molecules contribute alot to thermal conduction but not electrical conduction[10]. Furhter research on the field of organic electrolytes for thermocell applications should consider another salt, where the species that have high Eastman entropy also is redox active. Preferntially, the redox reaction should only involve an electron transfer and no products as water. Possibly, some metalorganic species with a metal ion that can have several oxidation states, is interesting for a thermocell.

Furhter work with the thermocell requires a better test cell.

6.3 Further work

Interesting directions for further work is to find new, more suitable electrolytes using organic solvents. Higher Seebeck coefficients can be obtained as the solvent and ionic species can be designed to have high Eastman entropy. Higher thermal resistivity can give the opportunity to use smaller electrode separation, yielding higher currents and smaller and lighter devices. It is believed that an electrolyte can be designed such that the redox reaction does not involve any undsired by-products as water. The first place to look should be metalorganic species, where a metal ion is coordinated by organic ligands.

Appendix A

ACNT density

$$\rho = \frac{mass}{volume} = \frac{mass}{AL}$$

When comparing samples with the same area A, we can use ρ' = ρ/A

$$\rho' = \frac{mass}{L}$$

For samples with same densities but different lenght, m_1 and m_2, L_1 and L_2, the realationship is

$$m_2 = m_1 \frac{L_2}{L_1}$$

For CNT on Al foil the mass can be represented as a funcition of % weight gain gain (w),

$$m_{cnt} = m_{Al}(w-1) = \rho_{Al} A t_{Al}(w-1)$$

t is thickness of the Al foil. Assuming uniform growth, then for two samples with different area a_1 and a_2

$$\rho_{A1} = \rho_{A2}$$

Then

$$m_{a1} = \rho_{Al} a_1 t_{Al}(w_1 - 1) \tag{A.1}$$

$$m_{a2} = \rho_{Al} a_2 t_{Al}(w_2 - 1) \tag{A.2}$$

By taking the ratio of A.1 and A.2

$$\frac{m_{a1}}{m_{a2}} = \frac{a_1}{a_2} \frac{w_1 - 1}{w_2 - 1} \tag{A.3}$$

The CNT density is uniform, and length the same, and

$$m_{a1} = a_1 L \rho \tag{A.4}$$

$$m_{a2} = a_2 L \rho \tag{A.5}$$

. The ratio A.5 and A.4 equals A.3, and w is independent of area.

When two samples have different ρ but same length L

$$\rho_1 = \frac{w_1}{w_2} \rho_2 \tag{A.6}$$

Appendix B

Double layer capacitance

The capacitance is given by

$$C = \frac{1}{v(V_f - V_i)} \int_{V_i}^{V_f} I(V) dV \tag{B.1}$$

The current I approximated as a linear function of voltage V, I = aV + b . b is set to 0, as when potential is unemployed there is no current.

$$C = \frac{1}{v(V_f - V_i)} \frac{a}{2} (V_f^2 - V_i^2) \tag{B.2}$$

For two electrodes, when V_f, V_i and v is similar, taking the ratio of equation B.2, we get

$$\frac{C_1}{C_2} = \frac{a_1}{a_2} \tag{B.3}$$

Appendix C

Arrhenius equation

The Arrhenius equation, k = rate constant, E_a is activation energy, A a constant, R is the gas constant and T is temperature. The rate constant using two different electrodes are equal at two different temperatures. The difference in activation energy can be found by solving B.1 with the conditions given in B.2.

$$k = Ae^{E_a/RT} \tag{C.1}$$

$$k_{NCNT}(T_1) = k_{CNT}(T_2) \tag{C.2}$$

$$E_{a,CNT} = \frac{T_2}{T_1} E_{a,NCNT} \tag{C.3}$$

Appendix D

Normalizaton of efficiency

Let j_B be the current density in the Baughman experiment, and j_N be the current density of the NCNT electrodes in this experiment. R_B is the thermal resistance in the Baughman experiment and R_N is the themal resistance of the cell in this project. Further

$$R = d/k$$

where k is thermal conductivity, which is similar for the two experiments. d is the electrode separation.

$$\eta = \frac{S_e j_{sc} R}{4}$$

By using the theoretical Seebeck coefficient, the ratio of the effciencies are

$$\frac{\eta_B}{\eta_N} = \frac{j_B R_B}{j_N R_N}$$

Now, by normalizing the current with respect to tube length/electrode thickness, and thermal resistance with respect to d

$$\frac{\eta'_B}{\eta'_N} = \frac{j_B/30 R_B/2.6}{j_N/1.7 R_N/2.2} = 0.048 \frac{\eta_B}{\eta_N}$$

This means that the normalized efficiency ratio is $0.048 \cdot 44.8 = 2.14$, hence the efficiency obtained by Baughman is 2.14 times the efficiency obtained in this project.

Bibliography

[1] T. amd Kanatzidis, Lyon, and Mahan, *Thermoelectric materials, new directions and approaches.* Materials research soc, 1997.

[2] D. M. Rowe, "Thermoelectrics, an environmentally friendly source of electrical power," *Renewable Energy*, vol. 16, 1999.

[3] T. J. Kang, S. Fang, M. Kozlov, C. S. Haines, N. Li, Y. H. Kim, Y. Chen, and R. H. Baughman, "Electrical power from nanotube and graphene electrochemical thermal energy harvesters," *Advanced Functional Materials*, vol. 22, 2012.

[4] S. B. Riffat and X. Ma, "Thermoelectrics: a review of present and potential applications," *Applied Thermal Engineering*, vol. 23, 2003.

[5] J. Li, T. C. A. Yeung, and C. H. Kam, "The upper limit of thermoelectric figure of merit: importance of electronic thermoelectric efficiency," *J. Phys. D Appl- Phys.*, vol. 45, 2012.

[6] B. R. Brown, M. Hughes, and C. Russo, "Thermoelectricity in natural and synthetic hydrogels," *Physical Review*, vol. 70, 2004.

[7] B. P. et al, "High thermoelectric performance of nanstructured bismuth antimony bulk alloys," *Science*, vol. 320, 2008.

[8] Boukai, Bunimovich, Tahir-Kheli, Yu, Goddard, and Heath *Nature*, vol. 451, 2008.

[9] R. Hu, B. Cola, N. Haram, Barisci, Lee, Stoughton, Wallace, Too, Thomas, Gestos, dela Cruz, Ferraris, Zakhidov, and R. H. Baughman, "Harvesting waste thermal energy using a carbon-nanotube-based thermo-electrochemical cell," *Nano Letters*, vol. 10, 2010.

[10] T. I. Quickenden and Y. Mua, "A review of power generation in aqueous galvanic cells," *J. Electrochem. Soc*, vol. 142, 1995.

[11] Tester, Holeschovsky, Link, and Corbett, "Evaluation of thermogalvanic cells for the convsersion of heat to electricity," 1992.

[12] M. Bonetti, S. Nakamae, M. Roger, and P. Guenoun, "Huge seebeck coefficients in non-aquous electrolytes," *The journal of chemical physics*, vol. 134, 2011.

[13] P. F. Salazar, S. Kumar, and B. A. Cola, "Nitrogen- and boron-doped carbon nanotube electrodes in a thermo-electrochemical cell," *Journal of The Electrochemical Society*, vol. 159, 2012.

[14] E. Eastman, "Electromotive force of electrolytic thermocouples and thermocells and the entropy of transder and absolute entropy of ions," *J.Am.Chem.Soc.*, vol. 50, pp. 283–292, 1928.

[15] C.H.Hamann, A.Hamnett, and W.Vielstich, *Electrochemistry*. Wiely-VCH, 1998.

[16] Melechoko, Merkulov, McKnight, Guillorn, and Klein, "Vertically aligned carbon nanofibers and related structures: Controlled synthesis and directed assembly," *J. App.Phys.*, vol. 97, 2005.

[17] E. Nuxualo and N. Coville, "Nitrogen doped carbon nanotubes from organometallic compounds: A review," *Materials*, vol. 3, pp. 2141–2171, 2012.

[18] C. et.al., "Identification of electron donor states in n-doped carbon nanotubes," *Nano letters*, vol. 1, 2001.

[19] S. Kundu, Xia, B. amd Becker, Schmidt, Havenith, and Muhler, "The formation of nitrogen containing functional groups on carbon nanotubes surfaces: a quantitative xps and tpd study," *Physical chemistry chemical physics*, vol. 12, pp. 4351–4359, 2010.

[20] A. H. Nevidomskyy, G. Csanyi, and M. C. Payne, "Chemically active substitutional nitrogen impurity in carbon nanotubes," *Phys.Rev.Lett.*, vol. 91, 2003.

[21] L. Li-Xiang, L. Yong-Chang, G. Xin, and A. Bai-Gang, "Supercapacitor from nitrogen-doped carbon nanotubes," *Advanced Materials Research*, 2011.

[22] J. W. Jang, C. E. Lee, S. C. Lyu, T. J. Lee, and C. J. Lee

[23] M. Kumar and J. Ando, "Chemical vapor deposition of carbon nanotubes: A review on growth mechanism and mass production," *Journal of Nanoscience and Nanotechnology*, vol. 10, 2010.

[24] N. Yoshikawa, T. Asari, N. Kishi, S. Hayashi, T. Sugai, and H. Shinohara, "An efficient fabrication of vertically aligned carbon nanotubes on flexible aluminum foils by catalyst-supported chemical vapor deposition," *Nanotechnology*, vol. 19, 2008.

[25] Noel and Vasu, *Cyclic Voltammetry and the frontiers of electrochemistry.* Aspect publications, 1990.

[26] Shriver and Atkins, *Inorganic Chemistry.* Oxford university press, 1999.

[27] J. E. B. Randles, "A cathode ray polarograph. part ii - the current-voltage curves," *Trans. Faraday Soc.*, vol. 44, 1948.

[28] S. Luidold and H. Antrekowitsch, "Hydrogen as a reducing agent: State-of-the-art of science and technology," *JOM*, vol. 59, 2007.

[29] Q. Li, X. Zhang, R. F. DePaula, L. Zheng, Y. Zhao, L. Stan, T. G. Holesinger, P. N. Arendt, D. E. Peterson, and Y. T. Zhu, "Nucleation and growth of carbon nanotubes by microwave plasma chemical vapor deposition," *Advanced Materials*, vol. 18, 2006.

[30] Bower, Zhou, Zhu, Werder, and Jin, "Nucleation and growth of carbon nanotubes by microwave plasma chemical vapor deposition," *Applied Physics Letters*, vol. 77, p. 2767, 2000.

[31] C. J. Lee, S. C. Lyu, Y. R. Cho, J. H. Lee, and K. I. Cho, "Diameter control of carbon nanotubes using thermal chemical vapor deposition," *Chemical physics letters*, vol. 341, 2001.

[32] F. Nitze, B. M. Andersson, and T. Waagberg, "Ammonia assisted growth of multiwalled carbon nanotubes," *PSS*, vol. 246, 2009.

[33] D. H. Lee, W. J. Lee, and S. O. Kim, "Highly efficient vertical growth of wall-number-selected, n-doped carbon nanotube arrays," *Nano letters*, vol. 9, 2009.

[34] J. Ting and S. Lin, "Growth and characteristics of carbon nanotubes obtained under different c2h2/h2/nh3 concentrations," *Carbon*, vol. 45, 2007.

[35] M. Picher, E. Anglaret, R. Arenal, and V. Jourdain, "Self-deactivation of single-walled carbon nanotube growth studied by in situ raman measurements," *Nano Letters*, vol. 9, no. 2, pp. 542–547, 2009. PMID: 19159251.

[36] E. D. Hondros, "Interfacial segregation of nitrogen in iron," *Metal Science*, vol. 1, 1967.

[37] F. Ohaski, G. Y. Chen, V. Stolojan, and S. R. Silva, "The role of the gas species on formation of carbon nanotubes during chemical vapor deposition," *Nanotechnology*, vol. 19, 2008.

[38] C. Brechignac, P. Houdy, and M. Lahmani, *Nanomaterials and Nanochemistry.* Springer, 2006.

[39] Puretzky, Geohegan, Jesse, Ivanov, and Eres, "In situ measurements and modeling of carbon nanotubes array growth kinetics during chemical vapor deposition," *Appl.Phys.A*, vol. 81, 2005.

[40] Wu, Huang, Ma, Huang, Liu, Yang, Chen, and Chen, "Distortion of carbon nanotube array and its influence on carbon nanotube growth and termination," *Colloids and Surfaces A: Physicochem. Eng. Aspects*, 2008.

[41] Y. Zhong and L.-S. L. et al, "Synthesis of high nitrogen doping of carbon nanotubes and modeling the stabilization of filled daato@cnts (10,10) for nanoenergetic materials," *Journal of Physics and Chemestry of Solids*, vol. 71, 2010.

[42] G. R. S. Iyer and P. D. Maguire, "Metal free, end-opened, selective nitrogen-doped vertically aligned carbon nanotubes by a single step in situ low energy plasma process," *Journal of materials chemistry*, vol. 21, 2011.

[43] J. Chen, Z. H. Zhu, S. Wang, Q. Ma, V. Rudolph, and G. Q. Lu, "Effects of nitrogen doping on the structure of carbon nanotubes (cnts) and activity of ru/cnts in ammonia decomposition," *Chemical Engineering Journal*, vol. 156, 2010.

[44] M. Baei, A. A. Peyghan, and M. Moghimi, "Theoretical study of cyano radical adsoprtion on (6,0) zigzag single walled carbon nanotube," *Chemical Monthly*, 2012.

[45] H. C. Jordi and J. E. Erman, "Cytochrome c peroxidase catalyzed oxidation of ferrocyanide by hydrogen peroxide. transient state kinetics," *Biochemistry*, vol. 13, 1974.

[46] B. amd Okotrub, Kurenya, Zhang, Zhang, Chen, and Song, "Electrochemical properties of nitrogen-doped carbon nanotube anode in li-ion batteries," *Carbon*, vol. 49, pp. 4013–4032, 2011.

[47] Harper, Stimson, and Abbott, "Voltammetry in non-aqueous solvents: Artefacts arising from slow electrolyte desorption," *Journal of Electroanalytical Chemistry*, vol. 520, pp. 6–12, 2001.

[48] S. S. Sekhon, "Conductivity behaviour of polymer gel electrolytes: Role of polymer," *Bull. Mater. Sci*, vol. 26, 2003.

[49] R. A. Rightmire, R. L. Rowland, and D. L. Beals, "Ethyl alcohol oxidation at platinum electrodes," *Journal of the electrochemical society*, vol. 111, 1964.

[50] Molodkina, Ehrenburg, Polukarov, Danilov, Souza-Garcia, and Feliu, "Electroreduction of nitrate ions on pt(1 1 1) electrodes modified by copper adatoms," *Electrochimica Acta*, vol. 56, 2010.

[51] Dima, Beltramo, and Koper, "Nitrate reduction on single crystal platinum electrodes," *Electrochemica Acta*, vol. 50, 2005.

[52] X. Yang, X. Wang, and J. Qiu, "Aerobic oxidation of alcohol over cabon nanotube-supported ru catalysts assembled at the interface of emulsion droplets," *Applied Catalysis A*, vol. 382, pp. 131–137, 2010.